Chemical Research in Toxicology

pubs.acs.org/crt

Article

In Vitro Toxicity Assessment of Pre- and Post-incinerated Organomodified Nanoclays on Airway Epithelial and Lung Fibroblast Cells

Todd A. Stueckle,* Jake Jensen, Jayme P. Coyle, Alixandra Wagner, Raymond Derk, Tiffany G. Kornberg, Sherri A. Friend, Molly Schreiner, Alexander C. Ufelle, Sushant Agarwal, Rakesh K. Gupta, Cerasela Zoica Dinu, and Liying W. Rojanasakul

Cite This: *Chem. Res. Toxicol.* 2025, 38, 1708−1728

Read Online

ACCESS | Metrics & More | Article Recommendations | Supporting Information

ABSTRACT: The use of two-dimensional organomodified nanoclays (ONCs) to improve nanocomposite properties continues to grow. Recent evidence suggests that airborne nanoclays in occupational environments pose an inhalation hazard; however, health risks and the underlying mechanisms remain undefined. In vivo studies evaluating pre- and post-incinerated ONC exposures found that cytotoxicity, inflammation, and fibrotic signaling responses are coating- and incineration status-dependent. We hypothesized that physicochemical property differences associated with coating presence/absence and incineration status of nanoclays will elicit changes in key events (KE) in exposed human small airway epithelial (SAECs) and normal lung fibroblast (NHLF) cells that contribute to pulmonary lung fibrosis. Using multiplex high-throughput screening strategies, SAEC and NHLF cells were acutely exposed (0−20 μg/cm^2) to pristine nanoclay (CloisNa), an ONC (Clois30B), their incinerated byproducts (I-CloisNa and I-Clois30B), and crystalline silica (CS), to evaluate how ONC characteristics influence several KE in the pulmonary fibrosis adverse outcome pathway. In vitro exposure to pre-incinerated nanoclay induced organic coating-dependent cytotoxicity in SAECs. CloisNa caused disruption of mitochondrial membrane potential, which coincided with loss in viability in both cell types. Clois30B exposure caused dose-dependent SAEC cytotoxicity, micronuclei formation, and mitochondrial hyperpolarization in SAECs and NHLFs. Incinerated nanoclays were noncytotoxic but elicited a SAEC mitochondrial radical and pro-inflammatory response. Direct in vitro exposure to NHLFs exhibited particle-dependent increased live cell count, reactive oxygen species production, and α-smooth muscle actin expression. Nanoclay-exposed NHLFs (0.6 μg/cm^2) possessed elevated collagen I levels while the same mass dose in vivo (300 μg/lung) favored elevated fibronectin and collagen III deposition for CloisNa and CS. In conclusion, organic coating presence and incineration status influenced nanoclays' effects on cellular interaction, membrane integrity, inflammation, fibroblast activation, and collagen accumulation in exposed cell models. Although pre-incinerated nanoclay exposure promoted collagen accumulation in vitro, it was a poor predictor of in vivo model reticular fiber deposition.

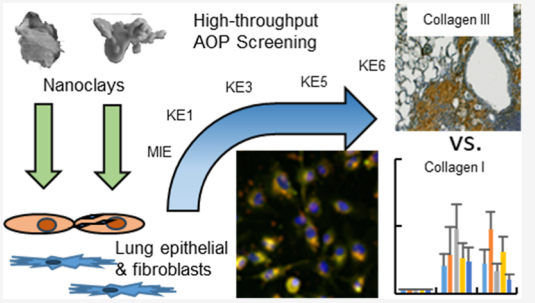

INTRODUCTION

Organomodified nanoclays (ONC), usually 2D smectite clays, are increasingly used in nanocomposite applications with a variety of different plastic matrices due to their strength, barrier function, and low flammability characteristics. Organic coatings, such as quaternary ammonium (QAC) and hydroxide, allow for the dispersion of smectite clays within matrices for a wide variety of applications. As such, ONC production continues to increase with market growth estimated at 9% to 13.3% and valued at $2 to $3.2 billion US by 2031.[1,2] Occupational exposures during manufacturing, handling, and use are known or largely expected to occur in the near future,[3] but limited evidence is available for airborne exposure levels (<39.2 mg/m^3) and resulting health risks.[4,5] Furthermore, ONC-containing materials experience either incineration or recycling upon disposal, thus raising the question of how incineration may alter released ONC characteristics, exposure, and resulting potential health risks.[6,7]

Inhalation of montmorillonite, a widely used natural smectite clay, causes inflammation, pneumonoconiosis, and silicosis-like lesions in Fuller's earth miners, which contain reticular fibers and little evidence for collagen deposition.[8−10] Silicosis is an irreversible lung disease characterized by

Received: May 22, 2025
Revised: August 29, 2025
Accepted: September 4, 2025
Published: September 19, 2025

https://doi.org/10.1021/acs.chemrestox.5c00206
Chem. Res. Toxicol. 2025, 38, 1708−1728

persistent silica particles, inflammation, and collagen deposition. The silica-induced inflammatory mode of action includes lysosome destabilization, NRLP3 activation, inflammatory cytokine release, and macrophage cell death, resulting in impaired clearance and chronic inflammation. In turn, this response drives fibroblast stimulation and extracellular matrix deposition.[11] This mode of action aligns with the current pulmonary fibrosis AOP in that particle interaction with resident pulmonary cell membrane components results in pulmonary fibrosis.[12] Currently, the underlying mechanism of montmorillonite "silicosis-like" response, however, remains undefined since these lesions notably possess a more reticular appearance in nature. Moreover, how QAC coating and incineration change the surface reactivity and the resulting airway and fibroblast responses in the lung fibrosis AOP remains elusive.

Nanomaterials are known to directly stimulate fibroblast activation, resulting in myofibroblast differentiation, proliferation, secretion of pro-fibrotic cytokines (e.g., TGFβ), and increased ECM synthesis and deposition. For example, direct CNT exposure to fibroblasts is thought to occur due to in vivo penetration to interstitial deposition and ECM production in both in vitro and in vivo models.[13] Nanosized CeO_2 was also shown to directly stimulate human fibroblasts in vitro, resulting in fibroblast proliferation, collagen I production, and fibrotic foci formation, which correlated with in vivo effects.[14,15] At present, it is unknown if montmorillonite and ONC direct stimulation of lung fibroblasts potentially contribute to ECM deposition and lung fibrotic response.

For nanoclays, few studies have attempted to investigate the latter half of key events in the lung fibrosis AOP including increased inflammatory mediators, loss of membrane integrity, fibroblast proliferation, and ECM deposition.[12] Studies to evaluate nanoclay inflammation and toxicity in pulmonary exposure models have reported that ONCs produce less inflammation, genotoxicity, and fibrosis in measured indices than pristine montmorillonite.[16,17] However, our laboratory's study did find pro-fibrotic signaling in pre- and post-incinerated ONC animals at 28 days post-exposure,[16] suggesting ONCs potentially possess fibrosis-causing characteristics. ONCs were shown to interact with airway epithelial, bronchial epithelial, and alveolar macrophage cells, resulting in elevated membrane damage, cytotoxicity, release of damage-associated molecular patterns, loss of monolayer resistance, DNA breaks, apoptosis, pro-fibrotic T_h2 signaling, and pyroptosis.[17−22] Acute exposures in in vitro studies suggest that coating and incineration status of nanoclay can determine cytotoxic potency, cell membrane and epithelial monolayer integrity, and the cell death mechanism in bronchial epithelial and macrophage cells.[18−21] Previously, we reported that coating and incineration status of ONCs impact the differentiated macrophage inflammatory and cell death mechanism following acute in vitro exposure and that these in vitro effects significantly correlate to acute BAL inflammatory cell infiltrate and inflammatory profiles in vivo.[18] Furthermore, preliminary evidence in a repeat nanoclay exposure in vivo model suggests that nanoclay platelets can deposit in the alveoli and possibly colocalize with interstitial fibroblasts,[23] suggesting the possibility of direct ONC and fibroblast interaction.

The main objective of this study was to evaluate how direct exposure of pre- and post-incinerated nanoclay to monocultures of human small airway epithelial and lung fibroblasts impact key events, namely, inflammation, membrane integrity, fibroblast activation, and extracellular matrix deposition, in the pulmonary fibrosis AOP. We hypothesized that direct nanoclay exposure would impact small airway epithelial cells' (SAEC) and normal human lung fibroblasts' (NHLF) cell viability, proliferation, membrane integrity, mitochondrial polarization, ROS generation, inflammation signaling, pro-fibrotic signaling, and ECM synthesis and that these effects would depend on nanoclay coating and incineration status. These studies would inform the latter key events within the lung fibrosis AOP for nanoclay along its lifecycle.

EXPERIMENTAL PROCEDURES

Particle Preparation and Characterization. Cloisite Na^+ and Cloisite 30B were acquired from Southern Clay Products (Gonzalez, TX). Incinerated Cloisite Na and Cloisite 30B (I-CloisNa and I-Clois30B) were produced by incinerating CloisNa and Clois30B particles as part of thermogravimetric analysis as previously described.[19] Heat-inactivated crystalline silica (CS; Min-U-Sil 5; US Silica, Berkeley Springs, WV) was used as a positive control particle for our studies based on similar crystal structure, surface properties, size, and morphology.[11,24] All characterization procedures of dry particles were previously conducted.[16,18,19]

Preparation of particle suspensions for characterization and cell exposures were conducted as previously described.[18] Briefly, 1 mg/mL particle stock suspensions were made in sterile Milli-Q water in sterile glass test tubes. Particle suspensions were sonicated three separate times (200.4 J/ml per run) with a cup horn sonicator (Sonics VibraCell VCX-750; Newton, CT) under cold water immersion with 1 min rest between sonication runs to achieve relative stable suspensions.[25]

Particle suspensions were immediately serially diluted in two different cell culture mediums: small airway growth medium (SAGM; Lonza, Walkersville, MD) and fibroblast growth medium 2 (FGM-2; Lonza). Each media's density, viscosity, and refractive index (Table S1) were determined using previously described methods (n = 3 independent experiments).[26] Particle density, packed pellet volume, medium density, and theoretical stacking factor (SF = 0.634) were used to calculate effective density (ρ_{EV}) of each particle (0.1 mg/mL) as previously described (n = 3).[26,27] Soluble endotoxin in sonicated stock suspensions (n = 3) was determined as previously described[16] and was below manufacturer-derived detection limits (<0.01 EU/mL).[18]

Since different cell culture media formulations can impact particle dispersion and stability, dynamic light scattering (DLS), particle dispersity index (PdI), and zeta potential analyses using were performed with a Zetasizer Nano ZS (Malvern, Malvern, UK) for each particle in water and culture mediums as previously described.[18] Briefly, DLS was performed to make relative size comparisons among medium and particle types and was not the sole technique for determining 2D particle size in suspensions.[28] Immediately after sonication, particles were diluted to 100 μg/mL and analyzed for size and zeta potential using a Universal Dip Cell (Malvern; n = 3). The pH of each particle suspension in each medium type was determined (n = 3) using a pH meter. Clois30B and both incinerated particles (I-CloisNa and I-Clois30B) were observed to reagglomerate and/or fall out of suspension in a low protein-containing medium;[16] therefore only the first runs off of each experiment were used for hydrodynamic diameter (Z_{avg}) and PdI analyses. Means and variability measurements were calculated for each end point.

FESEM Analysis of Particle Morphology and Size. To determine the morphology and accurately determine the particle size, dispersed particles were characterized and measured under S-4800 field emission scanning electron microscopy (FESEM; Hitachi, Tokyo) as previously described.[18] Briefly, sonicated suspensions of each particle in water were diluted in each culture medium (25−100 μg/mL), loaded onto filters, and sputter-coated for FESEM evaluation. Digital images were collected, and each particle was measured for maximum length and the corresponding 90° width in

https://doi.org/10.1021/acs.chemrestox.5c00206
Chem. Res. Toxicol. 2025, 38, 1708−1728

ImageJ. Individual particle diameter and length were measured per particle and medium type (n = 108−437). Size measurements of nanoclay particles in RPMI + 10% FBS medium from our previous study[18] were included to compare across medium types to further understand how different mediums and protein content determine dispersed nanoclay particle size under exposure conditions. 2−4 independent samples were prepared per particle and medium type.

Cell Culture. Human SAEC immortalized with human telomerase reverse transcriptase (hTERT; Lonza) were cultured in a Corning tissue culture-treated flask containing SAGM supplemented with a growth factor bullet kit as previously described.[29] Epithelial cells were used between passages 5 and 20. SAECs were chosen based on its long-term stability in culture, its ability to assess human airway epithelial response, and our laboratory's long-term use of this cell line for numerous engineered nanomaterial studies.[30−32] Cells were seeded at 5 or 10 × 10^3 cells per well in a 96-well plate overnight prior to exposure.

Primary NHLF, isolated from normal human lung tissue, were acquired from Lonza and cultured in a Corning tissue culture-treated flask from passages 2−8 in FGM-2 medium with growth supplements, including 2% FBS, fibroblast growth factor, and 1% penicillin/streptomycin. These cells were used based on our previous studies, showing that engineered nanomaterial (ENM) exposure caused proliferative and fibrotic-based responses, which correlated well with the in vivo mouse lung model.[14,33] Cells were seeded overnight at 5 × 10^3 and 3 × 10^5 in 96-well and 6-well plates, respectively, prior to exposure. Both SAEC and NHLF were passaged using trypsin and the trypsin inhibitor and reseeded in culture flasks according to the manufacturer's instructions.

To supplement the secreted cytokine assessment, THP-1 monocytes (ATCC, Gaithersburg, MD) were cultured in RPMI medium with 10% FBS and differentiated into attached macrophages as previously described.[18] Briefly, THP-1 monocytes were seeded at 1.5 × 10^5 cells per well in 6-well plates and then differentiated with Vitamin D_3 and PMA for 48 h. All cell cultures were maintained in a humidified incubator at 37 °C with 5% CO_2 air.

Particle Uptake Analysis. To ascertain the particle uptake into exposed cells, SAEC cells exposed to nanoclay particles were evaluated for particle uptake via TEM following published methods.[18,29] Briefly, SAECs were seeded at 7 × 10^5 in 6-well plates overnight and then exposed to test particles at 0.6 $\mu g/cm^2$ for 24 h. Cells were rinsed with saline wash, collected, and centrifuged to collect a pellet of the exposed cells. The pellet was resuspended in fixative, processed, blocked, sectioned, mounted, and imaged with TEM (JEOL 1400, Tokyo, Japan). 20−30 images were taken to evaluate the cellular uptake potential for each particle. Two independent experiments were performed for each particle.

To supplement the TEM analyses, enhanced dark-field microscopy (CytoViva, Auburn, AL) was used to help identify particle colocalization within different cell compartments. Sterile glass coverslips stored in 70% ethanol were placed in a 24-well plate, rinsed, and incubated for 24 h in SAGM to condition the glass surface. Next, SAECs were seeded at 3 × 10^4 per well in fresh warm SAGM for 24 h and then exposed to 0.6 $\mu g/cm^2$ for another 24 h. Next, cells were washed in HEPES saline, fixed 4% paraformaldehyde, and stained with HEMA3 (Fisher Scientific, Pittsburgh, PA) according to the manufacturer's protocol to maximize the visualization of Clois30B. Images at 60× and 100× were taken on a CytoViva-enabled Olympus scope with a DP73 camera. Four independent experimental runs were conducted.

WST-1 and LDH Assays. Assays were conducted as previously described[18] and according to the manufacturers' directions. Briefly, SAECs and NHLFs were seeded at 1 × 10^4 cells per well in quadruplicate overnight. Next, cells were exposed to each freshly sonicated particle at 0.02−20 $\mu g/cm^2$ in 200 μL (0.032−32 $\mu g/mL$) for 24 h. The highest dose models a 5 mg/m^3 respirable particle dose not otherwise regulated based on working lifetime exposure of 240 days per year for 45 years (OSHA PEL).[34] Cell free medium and 1% Triton-X served as blank and positive cytotoxicity controls, respectively. Next, plates were centrifuged followed by collection of 100 μL of the supernatant from each well for an LDH assay in a separate plate as a measure of cytotoxicity and loss of membrane integrity. 10 μL of the WST-1 reagent (Roche, Indianapolis, IN) and 100 μL of the LDH reagent (Roche) were added to cells and the supernatant, incubated for 2 and 0.5 h, respectively, and then absorbance read on each well with a microplate spectrophotometer (SpectraMax Plus 384, Molecular Devices, Sunnyvale, CA). An LDH interference assay was conducted as previously described[18] with data used to correct absorbance values from particle-exposed cell values (Table S2). Four independent experimental runs were performed.

High-Throughput Screening Analyses. Detailed methods on screening key events were previously reported.[18] Briefly, SAECs were seeded in 96- or 384-well black plates at 1 × 10^4 cells/well and exposed to a 0−20 $\mu g/cm^2$ applied dose. NHLFs were seeded in 96-well black plates at 5 × 10^3 cells/well. A two-way (5 particle x 8 dose) design for each time point was used with ≥quadruplicate replicates per treatment group. Cells were exposed for 0−48 h and then assayed using multiplex fluorescent staining panels and imaged at 4× to 40× magnification with the ImageXpress Micro XLS system (Molecular Devices). HTS key event end points using multiplex fluorescent staining assays are listed in Table 1. Each specific end point was chosen to align with the molecular initiating event or one of several key events (Table S3) as described in the pulmonary fibrosis adverse outcome pathway.[12] Assays were conducted following either dye manufacturers' recommendations or validated, standardized methods within our laboratory. Details on specific methodology are stated in the Supporting Information Methods. Multiplex fluorescent dye cocktails were prepared at 10× working concentrations along with 1 μM Hoescht 33342 as a nuclear stain. Following exposure, live cells were exposed to dye cocktails and incubated for 30−60 min and then subjected to live cell imaging on the ImageXpress system. If a high background signal was observed, cells were washed with fresh warm culture medium and imaged in warm, clear Fluorobrite DMEM (ThermoFisher, Pittsburgh, PA). One, four, nine, or 16 replicate sites were imaged per well at 4×, 10×, 20×, and 40× magnification, respectively. MetaXpress application modules (v6.2) or Custom Module Editor were used to quantitively measure cell parameter end points (e.g., dye intensity) and correct for background interference, noncell specific staining, and particle-only controls as previously described.[18,26,35] Corrected values were averaged within the site, replicate sites averaged within the well, and exported to statistical software programs from analysis. Three to four independent experimental replicates were executed.

Table 1. Key Event High-Throughput Screening Approach in Two Human Lung Cell Types following Pre- and Post-Incinerated Organomodified Nanoclay Exposure

AOP	stains and antibodies[a]	fluorescent channels
live/dead	propidium iodide	DAPI, Cy5
cell membrane damage[b]	LDH	n/a
cell metabolism[b]	WST-1	n/a
proliferation rate	propidium iodide	DAPI, TRITC (time course)
cell cycle	Ki67, p-HH3, EdU	DAPI, FITC, TRITC, Cy5
mitochondrial membrane potential	JC-1	DAPI, FITC, Cy3
mitochondrial ROS	MitoSOX Red	Cy5
intracellular reactive oxygen species	DCF	DAPI, FITC
micronucleus	propidium iodide	DAPI, Cy5
SAEC inflammation response	multiplex luminex beads	n/a
NHLF fibrogenesis[b]	n/a	n/a

[a]All HTS assays, except WST-1, LDH, and fibrogenesis, contained Hoechst 33342 as a nuclear stain. [b]Non-HTS traditional assays.

https://doi.org/10.1021/acs.chemrestox.5c00206
Chem. Res. Toxicol. 2025, 38, 1708−1728

Multiplex and ELISA Methods for Cytokine and Chemokine Release. SAECs were evaluated for release of inflammatory cytokines using a Luminex magnetic bead multiplex kit (R and D Biosystems, Minneapolis, MN) as previously described.[18] Briefly, cells were plated at 5×10^5 cells per well in 6-well plates and allowed to culture for 24 h. Cells were exposed to each particle (0−6 $\mu g/cm^2$) for 24 h ($n = 3$). Next, plates were centrifuged at 220*g* for 5 min to remove cell debris followed by collection of the conditioned medium in microcentrifuge tubes, which were stored at −80 °C until assayed. Samples were thawed on ice and assayed neat in duplicate on a 27-plex containing MIP-1α, MIP-1β, IL-1β, IL-2, IL-4, IL-5, IL-6, IL-8, IL-10, IL-7, IL-9, IL-12p70, IL-13, IL-15, IL-17α, IFN-y, IL-1ra, GM-CSF, Eotaxin, FGFβ, IP-10, G-CSF, MCP-1, PDGF-$\beta\beta$, RANTES, TNFα, and VEGF. Mean fluorescent intensities were calculated off a 7-point standard curve, averaged per treatment group, and tested for differences among treatment groups.

Literature suggests that platelet-derived growth factor released from several cell types, including fibroblasts and macrophages, plays a role in extracellular matrix remodeling in the damaged lung.[36−38] Separate PDGF-$\beta\beta$ and TGFβ ELISAs (R and D Systems) were conducted on conditioned medium from nanoclay-exposed NHLFs using the above-mentioned cell seeding (3×10^5 in a 6-well plate) and exposure procedures ($n = 3$). NHLF were exposed to the particulate (0−6 $\mu g/cm^2$) for 48 h ($n = 3$). Supernatants of the conditioned medium were collected, stored, and then assayed for human PDGF-$\beta\beta$ using the R and D Biosystems Duoset kit in duplicate. TGFβ samples were activated with HCl solution, neutralized, and assessed for TGFβ following the manufacturer's procedure in duplicate. To ascertain whether macrophages were a source of PDGF-$\beta\beta$ in nanoclay-exposed lung, human THP-1 monocytes were seeded at 1.5×10^5 cells per well and differentiated into macrophages using Vitamin D and PMA in 6-well plates as previously described.[18] Macrophages were exposed to the particulate (0−6 $\mu g/cm^2$) for 24 h ($n = 3$) in the absence or presence of lipopolysaccharide (LPS). The same PDGF-$\beta\beta$ procedure as above was used for macrophage supernatants. Results were compared to in vivo levels.

To compare in vitro to in vivo pulmonary responses following nanoclay exposure, we used a mass per unit alveolar surface area dose metric.[16] Previously, our study found that aspirated nanoclay and CS deposited in the terminal bronchioles, alveolar ducts, and surrounding alveoli. Administered in vitro doses of 0.06 and 0.6 $\mu g/cm^2$ equal in vivo doses of 30 μg/mouse and 300 μg/mouse, assuming 100% deposition in vitro and a 500 cm^2 alveolar epithelial surface area in a mouse lung.[39]

Correlation analysis of secreted PDGF-$\beta\beta$ levels comparing the in vitro macrophage to the in vivo BAL response was conducted on equal (0, 0.06, and 0.6 $\mu g/cm^2$) and 10× (0, 0.6, and 6 $\mu g/cm^2$) dose equivalents. Only CloisNa and Clois30B responses were evaluated since both incinerated nanoclays and CS did not produce significantly different responses in each model.

Animals. Analyzed animal tissues presented in this study were collected as part of a previously conducted study[16] evaluating the effects of oropharyngeal aspiration exposure of these same particles at 30 μg and 300 μg/mouse to the lungs of male C57Bl/6J mice (Jackson Laboratories, Bar Harbor, ME). The study was conducted in an AAALAC-accredited facility. The CDC-Morgantown Institutional Animal Care and Use Committee reviewed and approved all procedures for the animal study.

Fibroblast Activation and ECM Synthesis Comparison between In Vitro and In Vivo Models. NHLFs, seeded into 6-well plates overnight, were exposed to 0−0.6 $\mu g/cm^2$ to each particle for 48 h to evaluate changes in fibroblast activation and extracellular matrix protein expression. Exposed cells were held on ice, washed in cold PBS, and lysed on ice for 10 min with Invitrogen cell lysis buffer supplemented with a PMSF and protease inhibitor cocktail (ThermoFisher) as previously described.[16] Cell lysates were collected via a rubber policeman and micropipet, placed into an Eppendorf tube, and immediately frozen at −80 °C until assayed.

To evaluate both nanoclay-exposed in vivo lung tissue and in vitro NHLF ECM protein expression, total protein in Day 28 lung lysates ($n = 4$)[16] and NHLF lysates ($n = 4$) was determined using the BCA assay following manufacturer's instructions (Thermo Fisher Scientific). Briefly, 30 μg of protein for each sample was loaded onto 5% and 10% bis-acrylamide gel for SDS-PAGE analysis. Proteins were separated via electrophoresis in Tris glycine buffer and transferred to nitrocellulose membranes using a semidry transfer apparatus (Fisher Scientific) in tris buffer containing 20% methanol. A SNAP id 2.0 (MilliporeSigma, Burlington, MA) system was then used for all antibody incubations. Membranes were placed onto midi blot membranes and blocked with 0.5% nonfat dry milk in tris-buffered saline containing 0.1% Tween 20 (TBS-T) under suction. Next, each primary antibody, including collagen I (Fitzgerald, Acton, MA), collagen III, fibronectin, α-SMA (Abcam, Cambridge, MA), and β-actin (Sigma-Aldrich), was diluted and incubated twice for 10 min. Following suction, membranes were thrice washed with TBS-T and incubated with rabbit or mouse secondary HRP antibody for 10 min followed by suction. Membranes were again TBS-T rinsed, incubated with a HRP chemiluminescent substrate (MilliporeSigma), exposed to an X-ray film, and developed. Visible bands on films were digitally scanned and quantified using densitometry with ImageJ v1.52. Correlation analyses were performed on proteins that showed significant changes in vitro to the same protein in lung lysates at Day 28.

Fibronectin and Collagen III Immunohistochemistry. 5 μm fixed left lung tissue sections were placed on glass slides and subjected to immunohistochemistry staining for collagen III and fibronectin based on previously published methods.[40] Tissue sections for immunohistochemical analysis were deparaffinized and rehydrated xylene and graded alcohol, respectively. The antigen was retrieved by three microwave exposures (20% power for 5 min each) in citrate buffer (1 mM, pH 6.0) and then endogenous peroxidases quenched by incubation with 1% hydrogen peroxide for 10 min. The sections were blocked with 5% horse serum for 45 min, and then a rabbit polyclonal antibody against fibronectin (1:50 dilution, ab2413, Abcam) and a rabbit polyclonal antibody against collagen III (1 mg/mL, 1:50 dilution, ab7778, Abcam, Cambridge, MA) were applied separately on the samples and incubated overnight at 4 °C. Samples was then incubated in a biotinylated horse antirabbit secondary for 45 min at room temperature (1:200 dilution, BA-1100, Vector Laboratories Inc., Burlingame, CA). This was followed by incubation with the Vectastain Elite ABC reagent for 30 min according to the manufacturer's instructions (PK-6100, Vector Laboratories Inc.). DAB (brown) was used as the substrate according to the manufacturer's instructions (SK-4100, Vector laboratories Inc.). Finally, the sections were counterstained with hematoxylin. The primary antibody was replaced with 4% BSA in 1× PBS for the negative control slides. Images were taken using an Olympus AX70 microscope and DP73 camera. On average, nine random fields of view from three or four slides per treatment group were analyzed. Lung fibronectin and collagen III were quantified by binary color threshold pixel analysis using Nikon Elements analysis software (AR 5.02.00).

Statistical Analyses. All data sets were assessed for normal distribution of residuals and variance homoscedasticity ($\alpha = 0.05$) prior to conducting ANOVAs. Particle size differences between particle and medium types were determined by a one-way analysis of variance (ANOVA). Two-way ANOVAs were conducted to ascertain differences in SAEC and NHLF responses among the treatment groups. Linear mixed models were used to compare proliferation rates at different doses within the particle type. Cell phase data were analyzed with ggplot2 and other data processing packages in R (R Foundation for Statistical Programming, Vienna, Austria) as previously described.[35] MN data were analyzed by using a Kruskal−Wallis test. In vitro to in vivo correlation analysis was conducted on log-transformed data with Pearson's pairwise comparison tests. Fibronectin and collagen III IHC lung expression data were analyzed by using one-way ANOVA using GraphPad Prism software (version 7.05). All other data analyses were conducted in SAS JMP v15 software (Cary, NC).

https://doi.org/10.1021/acs.chemrestox.5c00206
Chem. Res. Toxicol. 2025, 38, 1708−1728

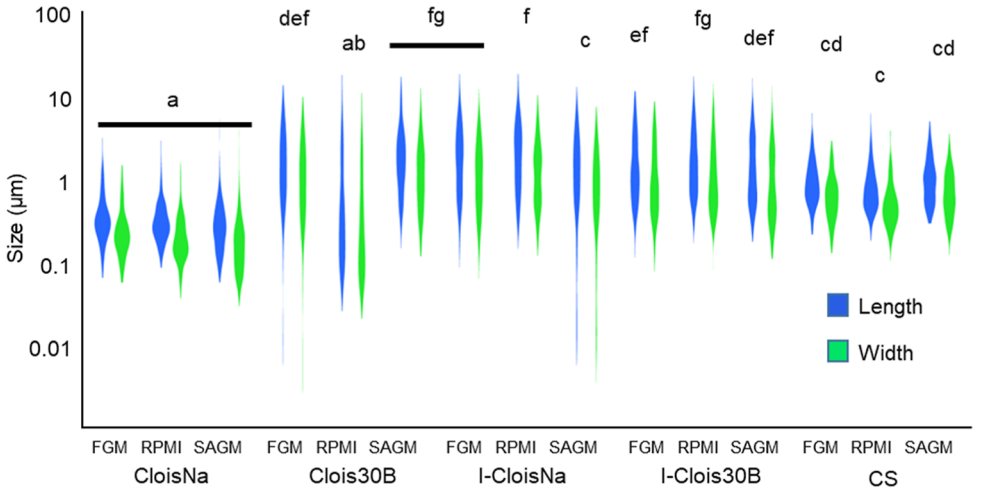

Figure 1. Nanoclay particle length and width distribution comparison in three different cell culture mediums. Sonicated particle suspensions were diluted to 25−100 μg/mL in each medium, filtered, and digitally imaged via FESEM. Different letters indicate those particle preparations that were significantly different from each other ($p < 0.05$; $n = 3$). Horizontal lines indicate those particles not significant from each other.

Table 2. Particle Characteristics of Pre- and Post-Incinerated Nanoclay in Two Different Lung Cell Culture Media[a,e]

	CloisNa	Clois30B	I-CloisNa	I-Clois30B	CS
SEM Morphology	small or large stacked platelets	small or large stacked platelets	smooth, amorphous	amorphous; pocketed; platelet-like	fractured, crystal-like
			SAGM		
SEM mean length (nm)	352 ± 25	2555 ± 194	1786 ± 171	1981 ± 121	1205 ± 77
SEM mean width (nm)	219 ± 17	1728 ± 136	1139 ± 124	1344 ± 88	839 ± 51
Z average (nm)	4198 ± 861[c]	1341 ± 399	3335 ± 1213	4211 ± 924[c]	1357 ± 63.3
PdI	0.381 ± 0.064	0.781 ± 0.049	0.783 ± 0.055	0.966 ± 0.035	0.619 ± 0.063
ζ	−13 ± 0.4	−11.1 ± 0.6	−11.7 ± 0.7	−10.9 ± 0.5	−9.8 ± 0.4
pH	7.58 ± 0.07	7.57 ± 0.01	7.08 ± 0.18	7.23 ± 0.09	7.52 ± 0.01
particle density ρENM (g/cm^3)	2.86	1.98	2.196[f]	2.65[f]	2.65
mean effective density ρEV (g/cm^3)[d]	1.065 ± 0.001^{A}	1.600 ± 0.030^{F}	1.312 ± 0.041^{BCD}	1.362 ± 0.015^{DE}	1.723 ± 0.044^{G}
			FGM-2		
SEM mean length (nm)	431 ± 40	2227 ± 171	2629 ± 176	2127 ± 36	1125 ± 78
SEM mean width (nm)	288 ± 24	1550 ± 124	1661 ± 110	1484 ± 24	752 ± 48
Z average (nm)[b]	305.7 ± 15.6	3870 ± 1509[c]	1309 ± 253	3448 ± 1263[c]	1032 ± 114
PdI[b]	0.236 ± 0.001	0.845 ± 0.102	0.836 ± 0.038	0.857 ± 0.076	0.475 ± 0.065
ζ[b]	−11.3 ± 0.6	−9.2 ± 0.4	−8.5 ± 0.4	−8.7 ± 0.4	−8.3 ± 0.3
pH[b]	7.11 ± 0.1	7.23 ± 0.08	7.48 ± 0.07	7.53 ± 0.06	7.41 ± 0.06
particle density ρENM (g/cm^3)	2.86	1.98	2.196[f]	2.65[f]	2.65
mean effective density ρEV (g/cm^3)[d]	1.080 ± 0.001^{A}	1.352 ± 0.018^{CDE}	1.424 ± 0.030^{E}	1.379 ± 0.012^{DE}	1.588 ± 0.027^{F}

[a]SEM values represent means ± 1 SE (n = 108−437). [b]Values represent means ± 1 SE of independent experiments (n = 3−6). [c]Value did not agree with SEM measurements. [d]A theoretical stacking factor of 0.634 was used to calculate ρEV. [e]Different capital letters indicate those ρEV significantly different from each other ($p < 0.05$). [f]Not determined; estimated density based on XRD data and.[127]

RESULTS

Nanoclay Dispersion and Uptake. Dispersed CloisNa in RPMI and FGM-2 media exhibited morphologies of single or stacked platelets similar to that observed in water, while dispersion in SAGM resulted in a mixture of single platelets, stacked plates, or large loose agglomerates of stacked platelets (Figures S1 and S2). CloisNa in all three medium types showed the significantly smallest mean length and width with medians ranging over 220−262 nm compared to all other particle and medium types (Figure 1 and Table S4).[18] DLS size data matched FESEM data, except for CloisNa dispersed in SAGM, which possessed a Z_{avg} of 4.2 μm. Regardless of medium type, CloisNa dispersed well (i.e., low PdI) and possessed the lowest ρ_{EV} of all particles tested (Table 2). Clois30B exhibited a range of size distributions, compared to CloisNa, and consisted of a small submicron or large single micron stacked platelet morphology in all three mediums. Clois30B particles in low protein media (i.e., SAGM and FGM-2) had a greater size (medians = 1672 and 1360 nm) than those in high protein RPMI medium (median = 304 nm). Similar to our previous observation,[16] Clois30B in water or low protein-containing medium was observed to slowly reagglomerate following sonication and suspension in the medium, resulting in larger agglomerates and enhanced particle deposition over time.

I-CloisNa possessed a smooth, amorphous quartz silicon oxide structure with an electron-dense, compact appearance

https://doi.org/10.1021/acs.chemrestox.5c00206
Chem. Res. Toxicol. 2025, 38, 1708−1728

(Figure S1). This differed from I-Clois30B's quartz silicon oxide structure, which exhibited morphologies including smooth, pocketed,[16,19] and platelet-like structures, albeit at significantly larger sizes than Clois30B. Incinerated particles showed comparable sizes across medium types, ranging from 1152 to 1955 nm, with suspension in SAGM causing the smallest particle size. DLS data were comparable to FESEM data except for larger Z_{avg} sizes for both particles in SAGM and I-Clois30B in FGM-2. Incinerated nanoclays showed minimal changes in ρ_{EV} ranging from 1.264 to 1.424 across all medias. Dispersed CS had a fractured, crystal-like morphology and displayed single micrometer sizes in all media, which was significantly smaller than both incinerated nanoclays and Clois30B in low protein-containing media. As protein concentration increased across the mediums, each particle's ρ_{EV} decreased or remained constant. Both Clois30B in SAGM and CS in SAGM and FGM-2 showed significantly higher ρ_{EV} values than all other particles in each media type.

Exposed SAECs displayed an uptake phenomenon similar to that previously observed in our THP-1 macrophage study, however, with some notable differences. CloisNa-exposed cells on occasion possessed large endosomes packed full of platelet structures to the point where the endosome membrane was barely recognizable (Figure S3, black arrows). A majority of Clois30B agglomerates were found inside endosomes or within the cytoplasm with no evidence of endocytic membrane. Both I-CloisNa and I-Clois30B were rarely observed in endosomes and were either acellular or found to be in contact with the cell plasma membrane. Enhanced darkfield microscopy supported the TEM analyses with both CloisNa and Clois30B colocalizing with the cytoplasm or in a perinuclear distribution (Figure S4). Both small and large size fractions of I-CloisNa, I-Clois30B, and CS were colocalized with the plasma membrane, cytoplasm, or the nucleus; however, manual Z plane adjustments during imaging suggested that these particles were deposited on top of the nucleus and not within the nuclear focal plane.

SAEC Viability, MMP, ROS, and Micronucleus Response to Nanoclay Exposure. Human SAECs were evaluated for nanoclay exposure-induced modes of action that would perturb normal lung airway epithelial cell health and function. A summary of results is presented in Table 3. Low doses of Clois30B (0.02−0.2 $\mu g/cm^2$) significantly increased SAEC cell number by 18% compared to unexposed controls, while only 0.02 $\mu g/cm^2$ CloisNa caused a similar effect (Figure 2A). Both incinerated nanoclays caused increased cell numbers from 0.02 to 6 $\mu g/cm^2$, while CS had no effect. Additional studies to confirm the particle-induced increased proliferation rate were conducted. Pre-incinerated nanoclays and I-CloisNa exposures (0.06−0.6 $\mu g/cm^2$) caused a significant increase in proliferation rate compared to unexposed cells (Figure S5 and Table S5). Both I-Clois30B and CS exposures exhibited nonsignificant increases in proliferation rate. Conversely, CloisNa caused significant loss of live cell at doses ≥2 $\mu g/cm^2$ while only 20 $\mu g/cm^2$ Clois30B, I-Clois30B, and CS caused a decrease of 57%, 17.5, and 25%, respectively (Figure 2A). Next, high doses of CloisNa (20 $\mu g/cm^2$) and Clois30B (≥2 $\mu g/cm^2$) significantly reduced cell viability (WST-1 assay) while only 20 $\mu g/cm^2$ of both CloisNa and Clois30B increased cytotoxicity as measured by LDH release (Figure 2B,C). I-CloisNa, I-Clois30B, and CS exposure had no effect on cell viability or cytotoxicity compared with unexposed cells.

Table 3. Summary of SAEC-hTERT and NHLF Cell Responses to Pre- and Post-Incinerated Organomodified Nanoclay Exposure[a,b,e]

end point	Clois Na	Clois 30B	I-CloisNa	I-Clois30B	CS
SAEC-hTERT					
Substance Interaction with Cellular Membrane Components (MIE)					
live cell count	↓↓↓	↑↑↓↓	↑↑	↑↑	NS
WST-1 viability	↓	↓↓↓	NS	NS	NS
Increased Pro-Inflammatory Mediators (KE1)					
MCP-1	↓↓	↓↓	↑↑	NS	↑↑
IL-6	NS	NS	↑	NS	↑
IL-8	↓↓	↓↓	↑↑↑	↑↑	↑↑
CCL5 (Rantes)	↓	↓	NS	NS	↑
Loss of Membrane Integrity (KE3)					
LDH cytotoxicity (%)	↑↑	↑↑	NS	NS	NS
MMP	↓↓↓	↑↓[c]	↑	NS	↑
MitoSOX Red	↓↓↓	↓↓↓	↑↑	↑↑	↑↑
CellROX Green	↓↓	↓↓	↓↓	↓↓	NS
proliferation rate	↑	↑	↑↑	NS	NS
cell cycle[c]	G1	G1, Go	S	S, G2	NS
Other End Points					
micronucleus (w/o block)	NS	↑↑	NS	↑	↑
micronucleus (w/block)	NS	NS	NS	NS	NS
NHLF					
Substance Interaction with Cellular Membrane Components (MIE)					
live cell count	↑↑ ↓↓↓[c]	↑↑ ↓↓↓[c]	↑↑	↑↑	NS
WST-1 viability	↓↓	↓↓	NS	NS	NS
Increased Pro-Inflammatory Mediators (KE1)					
TGFβ	↓↓	NS	NS	NS	NS
PDGF-$\beta\beta$	NS	NS	ND	ND	ND
Loss of Membrane Integrity (KE3)					
LDH cytotoxicity (%)	↑	↑↑	NS	NS	NS
MMP	↓↓↓	NS	NS	NS	NS
reactive oxygen species	↓↓↓	↓	NS	↑	↑↑
Fibroblast Activation/Proliferation (KE5)					
proliferation rate	↓↓	↓↓	NS	NS	NS
cell cycle[d]	NS	Go	NS	NS	NS
α-SMA expression	↑↑	↑↑	NS	NS	NS
Collagen Accumulation (KE6)					
collagen I expression	↑↑	↑↑	↑↑	↑	↑
pro-collagen III	NS	NS	NS	NS	NS
fibronectin	NS	NS	NS	NS	NS

[a]All data represent mean fold change compared to unexposed cells unless otherwise noted. [b]↑↑↑ large increase; ↑↑ moderate increase; ↑ modest increase; ↓↓↓ large decrease; ↓↓ moderate increase; ↓ modest increase; NS = not significantly different from unexposed control; ND = not determined. n/a = not applicable. [c]Order of arrows indicates increase at low dose (≤2 $\mu g/cm^2$) and decrease at high dose (≥6 $\mu g/cm^2$). [d]Indicates which cell cycle phases were observed to proportionally increase in exposed cells compared to unexposed cells. [e]n = 3−4 independent experiments.

CloisNa exposure at 6 $\mu g/cm^2$ caused increased proportion of cells in the G_1 phase while Clois30B at the same dose caused increased cells in G_0 and G_1 phase, indicating potential cell cycle arrest and alignment with a drop in viable cell number (Figure 2D). Conversely, I-CloisNa exposure caused a significant decrease in G_1 and increase in the S phase, while I-Clois30B exposure caused a significant increase in S phase cells, indicating potential proliferating SAECs correlating with

https://doi.org/10.1021/acs.chemrestox.5c00206
Chem. Res. Toxicol. 2025, 38, 1708−1728

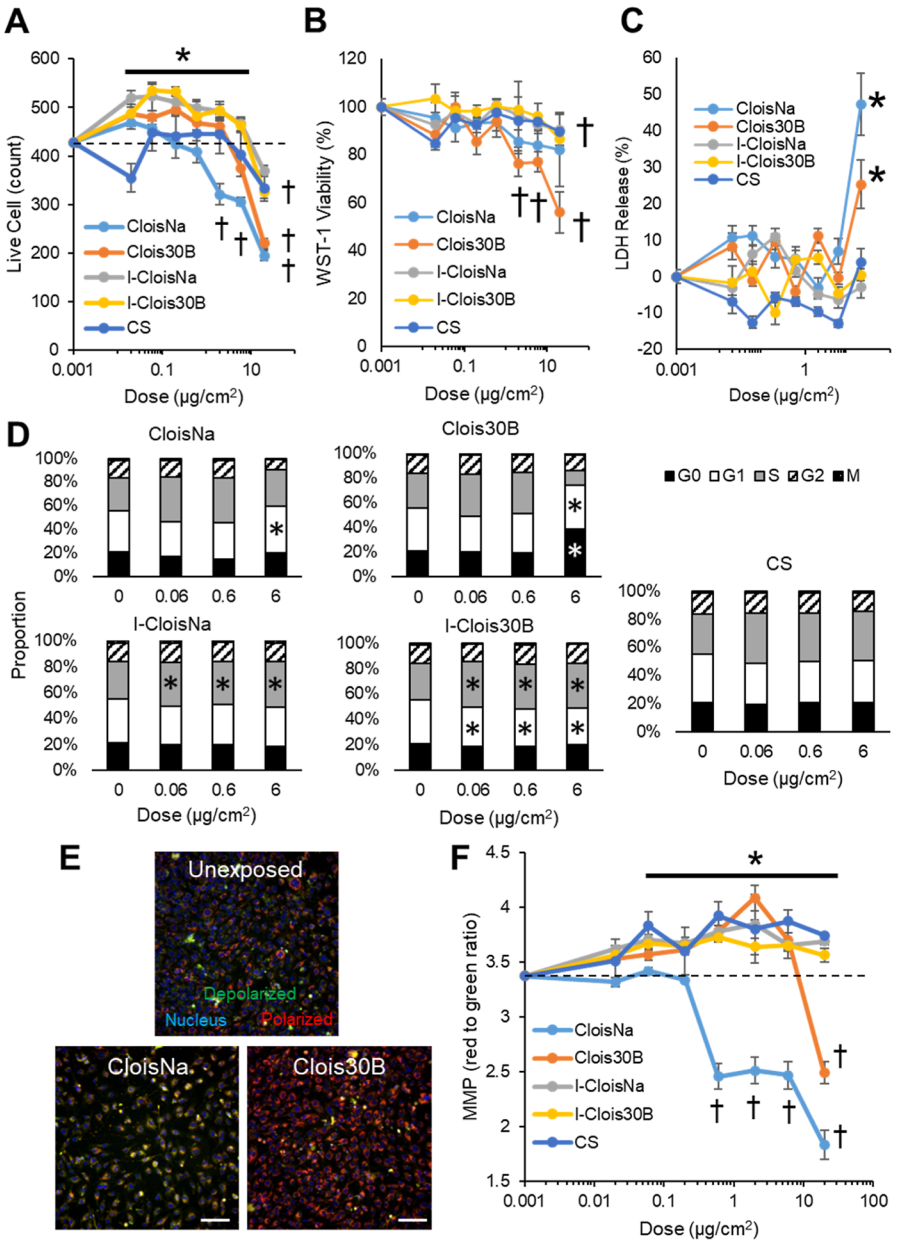

Figure 2. Automated high-throughput imaging analyses of human SAEC following pre- and post-incinerated ONC exposure at 24 h. CS served as a silica particle control. (A) Live cell counts via Hoechst 33342 and propidium iodide staining. (B) Cell viability measured by WST-1 assay. (C) Cytotoxicity measured by LDH assay. (D) Cell cycle and (E) representative fluorescent images of cells costained with JC-1 and Hoechst 33342. Scale bars represent 100 μm. (F) Mitochondrial membrane polarization response via JC-1 staining. Data represent means ± SE. Dashed horizontal line indicates unexposed control cell levels. * and † indicate treatments with significant increased or decreased responses, respectively ($p \leq 0.05$; n = 3−4 independent experiments).

live cell count and proliferation data. CS exposure caused no significant changes in the cell cycle at all tested doses.

Silica-containing particles are renowned for their ability to induce perturbations of mitochondrial function leading to increased ROS, membrane damage, and secretion of pro-inflammatory mediators, resulting in cell death or stimulation of pro-fibrotic signaling pathways,[11,41,42] which are established KEs in the pulmonary fibrosis AOP.[12] SAECs exposed to CloisNa (>0.6 μg/cm^2) exhibited a significant dose-dependent decrease in MMP that aligned with cytotoxic doses (Figures 2E,F and S6). Conversely, exposure to all other particles elicited subtle elevations in MMP that reached significance at 2 μg/cm^2, except for I-Clois30B. Higher doses of Clois30B reversed this trend with a significant decrease in MMP at 20 μg/cm^2 in cells with intact nuclei.

Given the inherent changes in MMP, SAECs were assessed for mitochondrial oxygen radical levels at 6, 12, and 24 h since perturbations to the mitochondria can alter such production.[43] Exposure to both pre-incinerated nanoclays for 12 h showed a dose-dependent drop in mitochondrial oxygen radical levels compared to controls, which coincided with cytotoxicity (Figure 3A). Conversely, both incinerated nanoclays and CS induced a significant elevation in mitochondrial oxygen radical levels at ≥6 μg/cm^2. No significant effects were observed at 6 and 24 h for all treatments. Preincubation with SOD resulted in no change in fluorescent MitoSOX red intensity, suggesting

https://doi.org/10.1021/acs.chemrestox.5c00206
Chem. Res. Toxicol. 2025, 38, 1708−1728

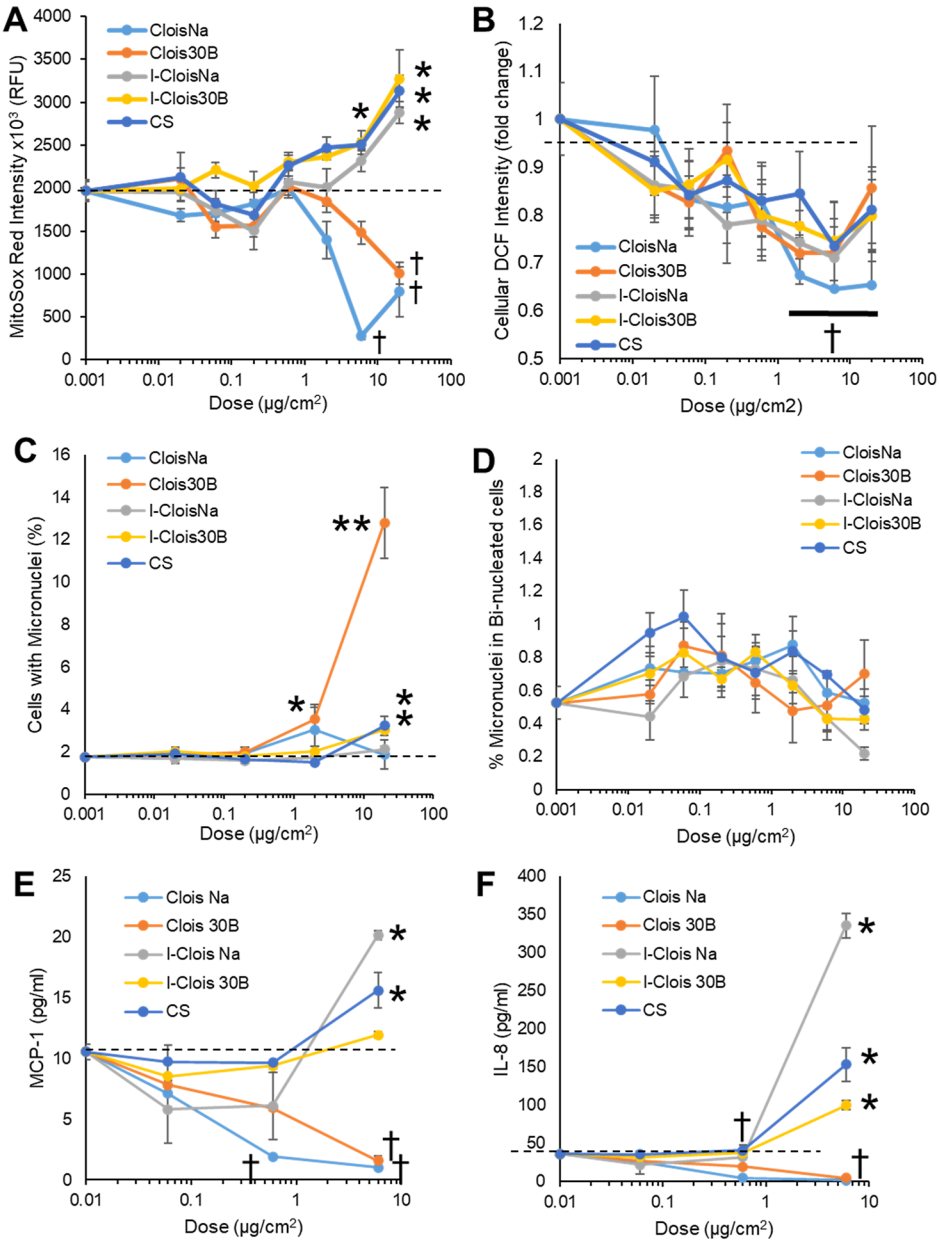

Figure 3. Reactive oxygen species (ROS), micronuclei, and inflammatory cytokine assessment in nanoclay-exposed human SAECs. CS served as a silica particle control. (A) MitoSOX Red and (B) intracellular ROS following nanoclay exposures at 12 and 24 h, respectively. (C) Percentage of surviving mononuclear and (D) binucleated cells with positive micronuclei following 48 h exposures. (E) Secreted MCP-1 and (F) IL-8 levels from human SAEC exposed to pre- and post-incinerated nanoclays for 24 h. Data represent means ± SE. The dashed horizontal line indicates unexposed control cell levels. * and † indicate treatments with significant increased or decreased responses, respectively ($p \leq 0.05$; n = 3−4 independent experiments).

that the superoxide ion was not responsible for the observed increase (Figure S7). SAECs exposed to all particles for 24 h, except CS, showed a significant decrease in reported ROS levels from 2 to 20 $\mu g/cm^2$. All other treatment groups showed moderate nonsignificant decreases in general ROS following 6 and 24 h exposure (Figures 3B and S8).

Previous in vitro analyses reported that ONC exposure can result in genotoxicity.[44,45] A micronucleus (MN) screening assay with no cytokinesis block found that 48 h exposure to Clois30B, I-Clois30B, and CS induced a significant increase in surviving SAECs containing single micronuclei ($X^2 \geq 6.3$; $p < 0.05$; Figure 3C). Clois30B possessed the strongest dose-dependent response with 2- and 7.3-fold increases in surviving SAECs at 2 and 20 $\mu g/cm^2$, while I-Clois30B and CS showed moderately significant increases at 20 $\mu g/cm^2$. Cytokinesis block MN assay results showed no significant difference in MN levels following exposure to all particles compared with unexposed controls (Figure 3D). Given that all particle-exposed cells ($\leq$6 $\mu m/cm^2$) maintained a proliferation rate above or at unexposed cell levels (Figures 2A and S5), these results suggest that Clois30B induced MN at 2 $\mu g/cm^2$ while 20 $\mu g/cm^2$ particle dose-induced MN were more due to cytotoxicity responses.

Incineration Status of Nanoclays' Influences Pro-Inflammatory Cytokine Secretion from SAECs. Both CloisNa and Clois30B induced significant dose-dependent

https://doi.org/10.1021/acs.chemrestox.5c00206
Chem. Res. Toxicol. 2025, 38, 1708−1728

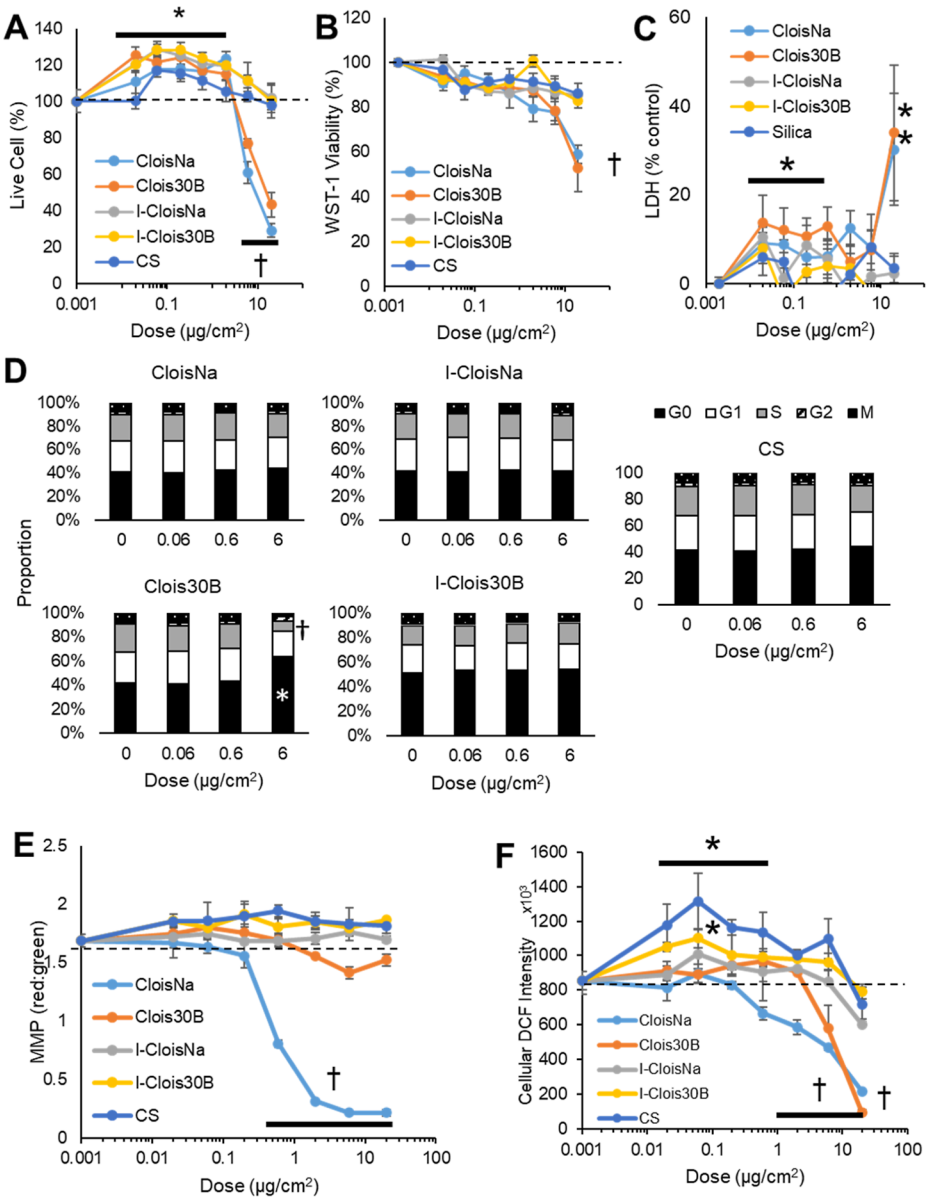

Figure 4. NHLF toxicological responses following acute 24 h exposure to nanoclays. (A) Live cell, (B) cell viability, (C) cytotoxicity, and (D) cell cycle shift analysis using the multiplex Edu, Ki67, and p-H3 assay. (E) CloisNa produced a dose-dependent loss in mitochondrial membrane potential. (F) I-Clois30B and CS caused increased intracellular ROS at moderate doses. * and † indicate treatments with increased or decreased effect, respectively, compared to unexposed control cells ($p \leq 0.05$, $n = 3-4$ independent experiments).

decreases in MCP-1, IL-8, and RANTES secretion compared to unexposed cells, coinciding with cytotoxicity (Figure 3E,F and Table S6). I-CloisNa and CS at 6 $\mu g/cm^2$ induced significantly increased MCP-1, IL-6, and RANTES secretion in SAECs, while both incinerated nanoclays and CS cause an increase in IL-8 secretion. All other 23 measured secreted cytokines showed no difference compared to unexposed controls (Table S6). Collectively, these results suggest that CloisNa and Clois30B exposures possess similar cytotoxic and inflammatory responses in SAECs, while CloisNa produces a MMP depolarization response and Clois30B causes enhanced membrane damage and MN formation in mononucleated cells. Lastly, incinerated particle exposure caused elevated SAEC proliferation and mitochondrial ROS at moderate doses and increased the ability to potentially recruit monocytes and neutrophils to exposed epithelium at high doses.

Nanoclay-Induced PDGF-ββ and Reticular Fiber Response in Human NHLF In Vitro and Mouse In Vivo Models. To evaluate the potential of nanoclay producing a direct fibrotic response, we exposed NHLFs to both pre- and post-incinerated ONC to evaluate their direct stimulation potential. Low to moderate doses (0.02−2 $\mu g/cm^2$) of all particles over 24 h, except CS, caused a significant increase in live cell count ranging from 18 to 29% above unexposed control cells, indicating potential cell proliferation (Figure 4A). Conversely, CS-exposed cells showed a significant increase ranging from 11 to 16% between 0.06 and 0.6 $\mu g/cm^2$. Both CloisNa- and Clois30B-exposed NHLFs showed decreased viability (WST-1 metabolism) at 20 $\mu g/cm^2$ (Figure 4B). Similarly, CloisNa showed increased cytotoxicity (LDH activity) at 20 $\mu g/cm^2$, but surprisingly, Clois30B elicited significantly elevated LDH levels (9 to 14%) compared to unexposed controls from 0.02 to 0.6 $\mu g/cm^2$ (Figure 4C),

https://doi.org/10.1021/acs.chemrestox.5c00206
Chem. Res. Toxicol. 2025, 38, 1708−1728

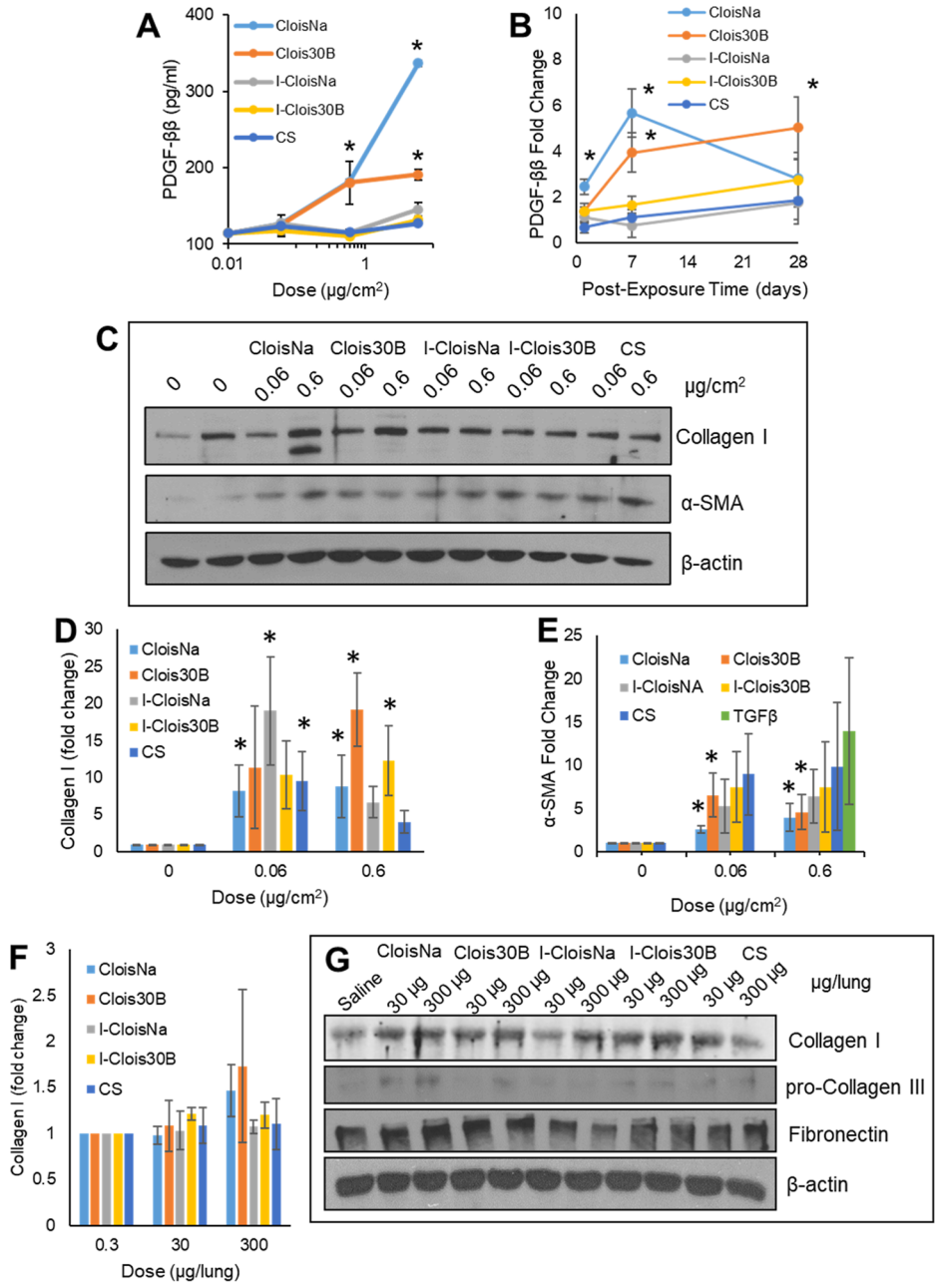

Figure 5. In vitro/in vivo comparison of pro-fibrotic response following pre- and post-incinerated ONC exposure. CS served as a silica particle control. (A) Human differentiated macrophage PDGF-$\beta\beta$ secretion following exposure to nanoclay. (B) In vivo PDGF-$\beta\beta$ at Day 7 correlated with macrophage in vitro response (C−E) NHLF Collagen I and α-SMA expression at in vitro dose equivalents to those used in an in vivo aspiration exposure model following 48 h exposure. TGFβ at 1 ng/mL served as a positive control in all experiments. Bars represent the mean ± SE with n = 3−4. (F and G) Extracellular matrix proteins associated with pro-fibrotic and/or reticular fiber genesis following in vivo aspiration exposure in C57BL/6 mouse lung at Day 28 (n = 4). * indicates significant differences compared to the control using either ANOVA or Wilcoxon X^2 tests ($p \leq 0.05$; n = 3−4 independent experiments).

indicating moderate damage or increased leakiness of NHLF membranes at doses shown to stimulate NHLFs. All other particle treatments had no significant effect on cell viability or cytotoxicity compared to controls.

The fibroblast proliferation rate did not significantly increase above unexposed controls for any particle or dose combination ($p > 0.05$; Figure S9 and Table S7). Rather, 6 μg/cm^2 of both CloisNa and Clois30B significantly decreased the proliferation rate compared to all other doses. Likewise, cell cycle analysis showed no changes in proportion of cells in each phase for all particle exposure groups, except for 6 μg/cm^2 Clois30B-exposed cells that displayed a significant decreased proportion of cells in the S phase with an increased proportion in the G_0 phase (Figure 4D).

Next, only CloisNa exposure caused dose-dependent MMP depolarization (≥0.6 μg/cm^2; Figure 4E) while all other treatments had no effect. The MMP decrease in CloisNa-exposed cells coincided with a decrease in intracellular ROS at ≥2 μg/cm^2 (Figure 4F). Clois30B exposure caused a loss of intracellular ROS at 20 μg/cm^2 only. Conversely, I-Clois30B (0.06 μg/cm^2) and CS exposure (0.02−0.6 μg/cm^2) caused a significant elevation in intracellular ROS while all other

https://doi.org/10.1021/acs.chemrestox.5c00206
Chem. Res. Toxicol. 2025, 38, 1708−1728

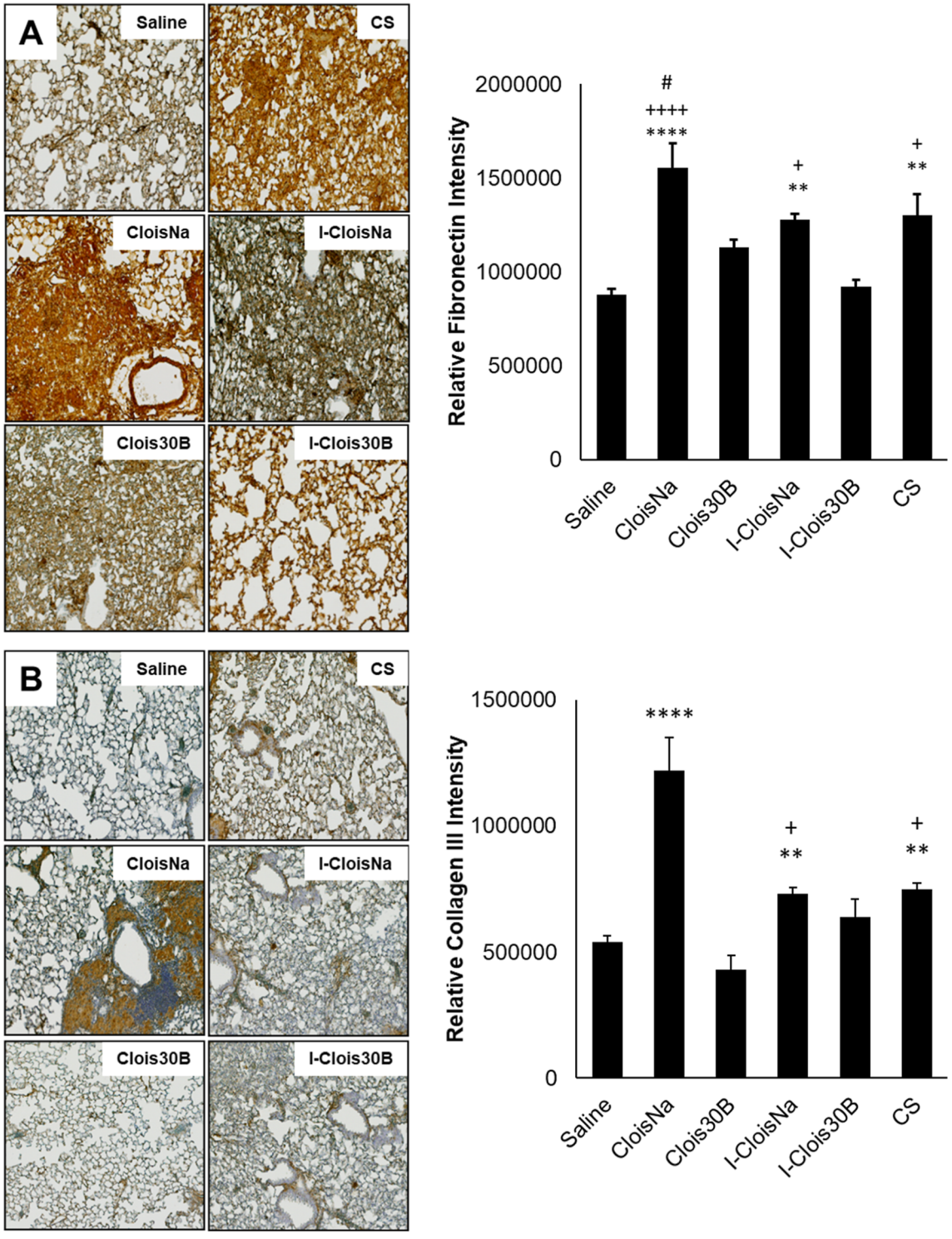

Figure 6. Immunohistochemical staining of reticular fiber matrix in pre- and post-incinerated ONC-exposed (300 μg) in male C57BL/6J mouse lung at Day 28. (A) Fibronectin and (B) collagen III in lung tissue with representative images (left) and relative intensity quantification (right). Saline and CS served as vehicle and positive controls, respectively. Low dose animal data not shown. n = 3−4 per group. ** and **** indicate p < 0.01 and p < 0.0001 vs saline control, respectively. + indicates p < 0.05 vs I-Clois30B-exposed mice, # indicates p < 0.05 vs CC-exposed mice by one-way ANOVA followed by the Bonferroni correction for multiple comparisons.

treatments had no effect. Collectively, pre-incinerated nanoclays caused cytotoxicity through potentially two different modes of action (mitochondrial vs cell membrane damage), while low doses caused increased cell number. Post-incinerated nanoclay exposure had no effect on NHLF while CS moderately increased intracellular ROS.

Based on this evidence for direct NHLF activation, we assessed pro-fibrotic markers and extracellular matrix/reticular fiber protein expression in exposed NHLF and compared to dose-equivalents (0.06 and 0.6 μg/cm^2 vs 30 and 300 μg/lung) in an exposed C57Bl/6 mouse lung. No significant increase in secreted PDGF-$\beta\beta$ and TGFβ levels at 48 h in NHLF was

https://doi.org/10.1021/acs.chemrestox.5c00206
Chem. Res. Toxicol. 2025, 38, 1708−1728

observed following all particle treatments. Rather, CloisNa exhibited a dose-dependent decrease in TGFβ that coincided with NHLF's loss in MMP (Figure S10). In macrophages, however, exposure to both pre-incinerated nanoclays resulted in a dose-dependent significant increase in secreted PDGF-$\beta\beta$, with CloisNa exhibiting greater potency at 20 μg/cm^2 (Figure 5A). This trend correlated with PDGF-$\beta\beta$ levels measured in BALF from C57BL/6 mice at Day 7 post-exposure to 300 μg,[16] but not on Day 1 or Day 28 (Figures 5B and S11). A 10× in vitro dose equivalent showed no significant correlations to the in vivo dose.

Next, both CloisNa and Clois30B exposures showed a dose-dependent increase in NHLF α-SMA, with Clois30B showing enhanced potency at lower doses (Figure S12). CloisNa exposure caused a significant increase in NHLF collagen I expression, while all other particles caused dose-specific increases compared to unexposed cells (Figure 5C,D). NHLF α-SMA expression was significantly increased following both pre-incinerated nanoclay exposures, while both post-incinerated nanoclays and CS showed a nonsignificant increase compared to unexposed controls (Figure 5E). Comparatively, no significant increase in collagen I (Figure 5F,G; $p > 0.05$) and α-SMA expression (data not shown; $p > 0.05$) was observed in mouse lung at Day 28 post-exposure compared to unexposed animals. However, correlation analysis revealed a significant correlation between the equivalent high dose in vitro (0.6 μg/cm^2) to in vivo (300 μg/lung) of collagen 1 expression ($r = 0.87$; $p = 0.025$; Figure S13). An equivalent low dose (0.06 μg/cm^2 vs 30 μg/lung) showed no correlation ($r = 0.20$; $p > 0.05$). Moreover, no correlation existed between in vitro and in vivo α-SMA expression levels at either dose equivalent comparisons. Given the known reticular fiber deposition following long-term montmorillonite inhalation exposure,[8,10,46] both fibronectin and collagen III expressions were evaluated in both in vitro and in vivo models. NHLFs in culture showed no change in both fibronectin and collagen III expression for all particle treatments (not shown; $p > 0.05$). In vivo expression of soluble protein in homogenized whole lung showed nonsignificant moderate increases in fibronectin and pro-collagen III for CloisNa and fibronectin in Clois30B at Day 28 post-exposure compared to a saline-exposed lung (Figure 5G). Both incinerated nanoclays and CS showed no significant change.

Based on pathological findings of CloisNa induction of granulomatous lung lesions and pro-fibrotic cytokine signatures in lung BALF,[16] we evaluated nanoclay-exposed lung tissue exposed to 300 μg for fibronectin and collagen III deposition via IHC staining. Quantitative analysis of stained lung sections found that a high dose of CloisNa caused a significant 1.8- and 2.3-fold increase in fibronectin and collagen III deposition, respectively (Figure 6A,B). Clois30B showed only a 1.3-fold nonsignificant increase in fibronectin. I-CloisNa- and CS-exposed lung experienced a significant 1.4-fold increase in both proteins while I-Clois30B only showed minimal increases. Collectively, direct in vitro acute exposure of NHLF to moderate doses of pre-incinerated ONC caused elevated live cell counts, α-SMA expression, and collagen I expression. The in vitro extracellular matrix production of collagen I correlated only with in vivo production of collagen and no other reticular fiber proteins.

DISCUSSION

Based on these collective results, we concluded that nanoclay coating and incineration status impacted SAEC and NHLF viability, proliferation, inflammation signaling (KE1), loss of membrane integrity (KE3), mitochondrial health, fibroblast activation (KE5), and ECM synthesis (KE6) following exposure. A comparison analysis between in vitro vs in vivo ECM synthesis following nanoclay exposure found no correlation in the type of major ECM components, suggesting that direct nanoclay exposure to a NHLF monoculture is not predictive of an in vivo response. This study provides key information about how physicochemical differences of montmorillonite nanoclay along its lifecycle influence KEs in the pulmonary fibrosis AOP (Figure 7).

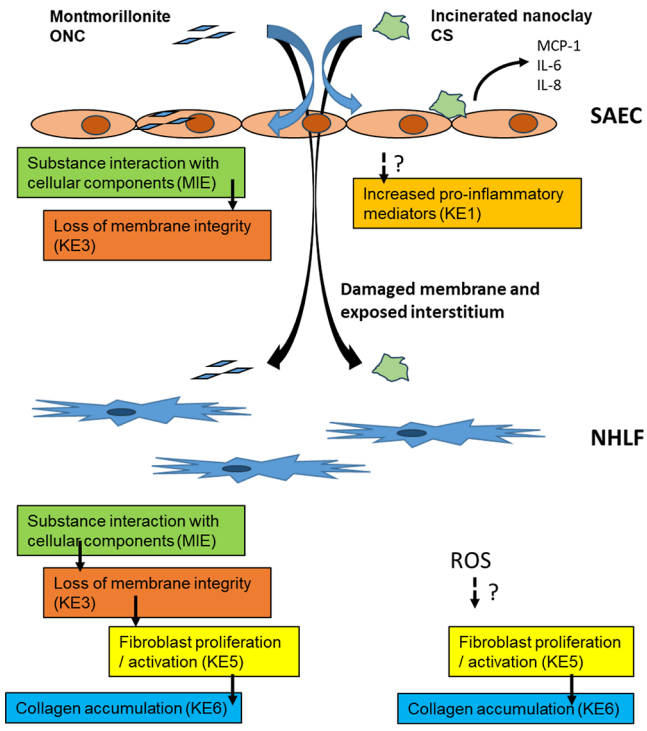

Figure 7. Proposed AOP for direct nanoclay exposure to terminal bronchiole and underlying interstitial fibroblasts. Acquired data supported the molecular initiating event (MIE) and several key events (KE) within the AOP.

High doses of pre-incinerated nanoclay were clearly toxic to both cell types; however, noticeable potency differences between CloisNa and Clois30B exposure responses (i.e., live cell, WST-1 viability, proliferation rate) were observed, indicating that the absence or presence of the QAC coating influenced toxicological responses. An interesting difference was observed in SAECs with CloisNa significantly reducing live cell counts at fairly low doses, possibly due to a combination of its lytic ability, higher surface area,[47] and mitochondrial depolarization ability, while Clois30B and both incinerated nanoclays significantly increased live cell count above unexposed controls. These effects coupled with clear nanoclay particle uptake and interaction with endosomes align with the MIE (Figure 7). Proliferation rate comparison analysis displayed a similar trend. The proliferation finding contradicts previous reports that ONCs and incinerated nanoclays are primarily cytotoxic and/or have no proliferative effect.[19,20,48]

https://doi.org/10.1021/acs.chemrestox.5c00206
Chem. Res. Toxicol. 2025, 38, 1708−1728

This is potentially due to previous studies' use of tetrazolium assays that measure metabolism and not cell count, high dose ranges, and differences between cell models. Interestingly, we did detect a moderate increase in LDH activity in Clois30B-exposed NHLFs, which indicated disruption to the fibroblast plasma membrane (KE3). Several studies reported that nanoclays (including bentonite, montmorillonite, and laponite) interact with lipid monolayers and lung surfactant, resulting in changes of the biophysical properties of those layers, resulting in potential adverse impacts to resident lung cells.[49−51] Additionally given that both CloisNa and Clois30B experienced uptake with apparent interaction with endosome membranes in both SAECs and THP1 macrophages along with alarmin release (IL-1α and ATP) in THP1 macrophages,[18] our collective findings lend additional evidence to both uncoated and organomodified montmorillonite interacting with resident pulmonary cell membrane components, which is the MIE in the pulmonary fibrosis AOP (Figure 7).

Surprisingly, immortalized SAECs were tolerant of pre-incinerated ONC exposure, with measures of toxicity only observed at the highest doses, while uncoated montmorillonite displayed a greater degree of cell death at subacute cytotoxic doses. Moreover, these findings indicate that pre-incinerated montmorillonite exposure causes loss of membrane integrity (KE3, Figure 7). Our previous comparison of three different QAC coatings on Nanomer and Cloisite nanoclays showed the methyl dihydroxyethyl hydrogenated tallow ammonium coating, same coating as Clois30B, showed the greatest amount of cytotoxicity to both BEAS-2B and primary SAECs (IC_{50} = 2.1 and 0.5 $\mu g/cm^2$, respectively) compared to uncoated, octadecylamine with an aminopropyltriethoxysilane coating, and dimethyl dialkyl amine coating nanoclays.[19,20] Exposure to these same Nanomer ONCs at their respective IC_{50}s, regardless of coating, showed moderate ability to disrupt human bronchial epithelial monolayer integrity with apparent recovery through time.[21] This study's finding of proliferation at subtoxic Clois30B doses could explain the apparent recovery of epithelial cell monolayer recovery following ONC exposure where surviving cells experience mitochondrial hyperpolarization, potential increased energy production, and increased proliferative capacity. Other studies reported tallow QAC coatings with dimethyl benzyl hydrogenated or long alkyl chain with hydroxl groups possessing stronger cytotoxic potential,[20,52,53] suggesting that long chain or complex functional groups on cationic ammonium QAC coatings are more cytotoxic to human lung epithelial cells than short chain or uncoated nanoclay. At present, it is unclear if QAC coatings experience differential solubilization, reactivity, or chemical modification that depends on the cell culture medium. Several additional reasons to explain these conflicting results include larger particle sizes in the SAGM medium, hTERT immortalized SAECs possessing greater tolerance for Clois30B, and greater susceptibility to uncoated montmorillonite than primary cells possibly via altered p53 stress response and apoptosis regulation,[30,54] differences in well plating densities, and well plate size.

High dose pre-incinerated nanoclay exposure caused a G_1 shift while low to moderate doses of incinerated nanoclay caused a S and G_2 shift. Previously, very few studies evaluated bentonite, montmorillonite, or ONC impacts on cell cycle shift, which is surprising given their known toxicities. In vitro montmorillonite exposure to several different cancer cells resulted in G_0/G_1 or S-phase arrest, which coincided with Cyclin D reduction, overexpression of mTOR, and apoptosis or autophagy-mediated cell death.[55] Both montmorillonite and ONC in vitro exposures are known to cause DNA damage (i.e., Ames mutagenesis, micronuclei, DNA strand breaks) at an in vitro high dose, in bronchoalveolar lavage cells following installation, and human workers under high exposure conditions, thus causing potential arrest at G_1 or S-phase cell cycle checkpoints.[5,17,44,48] Significant cell cycle shifts did not occur until cytotoxic pre-incinerated nanoclay doses, suggesting either cell death or DNA damage mechanisms were occurring.

Amorphous and CS exposure can cause cell cycle shifts, S-phase, or G_2/M phase arrest in response to elevated oxidative stress or DNA damage.[56−59] Brandão et al.[60] reported that nanosized amorphous silica caused a significant shift of rat alveolar cells from G_1 to S and G_2/M phases, which aligns with our findings. Our previous study reported that incinerated nanoclay from a polylactic acid composite caused initial moderate damage to the epithelial monolayer and no significant effect on BEAS-2B cell cycle phase, which allowed for recovery and monolayer re-establishment.[61] Given the significant and nonsignificant increases in proliferation rate following incinerated nanoclay exposure, the observed cell cycle shift at the similar doses is more likely to support cell proliferation than a cytotoxic mechanism (i.e., ROS, DNA damage). Collectively, these findings indicate that pre- and post-incinerated nanoclay exposure can result in interaction with lung epithelial cellular components (MIE), loss of membrane integrity (KE3), and proliferation (Figure 7). Future studies should evaluate whether the epithelial-to-mesenchymal transition is involved in lung epithelial monolayer response and wound repair.

Altered MMP, as a source of ROS, along with intracellular and mitochondrial ROS were assessed due to the established role of oxidative stress (as part of KE3) contributing to the inflammation, epithelium injury, and fibroblast activation KEs in the pulmonary fibrosis AOP. CloisNa exposure ($\geq$0.6 $\mu g/cm^2$) caused significant loss of MMP in both tested cell lines and differentiated THP1 macrophages,[18] lending further evidence that mitochondria are a toxicological target of montmorillonite following inhalation exposure. Excessive mitochondrial depolarization can lead to increased ROS, loss of adequate ATP generation, and eventual cell death.[43] Here, it appears that MMP loss coincided with cytotoxicity but with no mitochondrial or intracellular ROS increase. Studies report that some silica particles can produce ROS, which leads to mitochondrial damage, mitophagy, and cell death,[62] while others report that silica damages the electron transport chain, depolarizing mitochondria, increasing ROS, and leading to cell death.[63] Alternatively, silica particle uptake in phagolysosomes was shown to generate short-lived ROS, phagosome leakage, elevated MMP, and moderate cytoplasmic ROS in the first few hours of particle uptake, which collectively lead to apoptosis. Later time points showed a drop in MMP with no detectable ROS.[64,65] Mild depolarization due to partial mitochondrial uncoupling can protect cells against mitochondrial reactive oxygen species generation.[66] These later studies better align with our findings with CloisNa exposure to SAECs, suggesting a short-lived ROS or non-ROS-induced cytotoxicity mechanism. Compared to differentiated THP-1 macrophages, SAECs and NHLF were more sensitive to CloisNa in intracellular ROS response, while no major differences were observed for all other particles. No substantial differences were observed

https://doi.org/10.1021/acs.chemrestox.5c00206
Chem. Res. Toxicol. 2025, 38, 1708−1728

between depolarization of mitochondria or intracellular ROS in exposed macrophages.[18] Differences in sensitivity are potentially due to the biocorona protective effect (i.e., high protein containing [THP-1 cells] vs low protein-containing [SAEC and NHL medium]), underlying phagocytic ability, and tolerance for phagocytosed particles.[67,68]

Alternatively, low-dose Clois30B exposure hyperpolarized mitochondria in SAECs, with no apparent effect observed on the MMP in NHLFs. This finding adds to previous studies that identified Clois30B and other cationic QAC exposures target the mitochondria.[53,69−72] At present, it is unclear whether soluble QAC from Clois30B,[73,74] the ONC particle itself, or a combination of the two caused this effect.[52] Acute mitochondrial hyperpolarization may indicate a stress response with enhanced energetic demands due to mild proliferation associated with low to moderate ONC exposure while prolonged hyperpolarization coincides with increased autophagy, reduced apoptotic signaling, and inflammasome activation.[75] Epithelial proliferation may also explain our group's previous finding that moderate exposure to an ONC with similar QAC coating resulted in quick monolayer recovery following exposure and increased monolayer resistance over time compared to unexposed controls.[21] Alternatively, hyperpolarization of mitochondria is associated with elevated ROS, and an early, but reversible step in apoptosis, autophagy, and ER stress[76] and is reported following amine-coated particle exposure.[77]

Incinerated nanoclay and CS exposure caused elevated mitochondrial ROS in SAECs, with subsequent low intracellular ROS levels, compared to unexposed controls, suggesting that tested cell types experienced short-lived ROS production and retained their protective antioxidant capacity. These findings align with our previous studies with post-incinerated nanoclays that showed low toxicity compared to pre-incinerated particle and that cytotoxic doses indeed cause elevated ROS and apoptosis in human lung epithelial cells at ≥20 μg/cm.[2,19−21] Another study comparing fumed silica against colloidal and Min-U-Sil 5 silica found that fumed silica, with silanol groups on three-membered rings, drives hydroxyl formation, ROS generation, and cytotoxic effect in BEAS-2B cells.[78] Conversely, a separate study argues that high-temperature-flame-generated silica with low silanol content produced high amounts of short-lived abiotic ROS, cytotoxic effects in macrophages, no intracellular ROS, and no cytotoxic effects on human SAECs.[79] Differences in size, surface area, synthesis conditions, silanol content, and the in vitro cell model are thought to contribute to differences in amorphous silica toxicity.[11,36,79] Alternatively, different classes of radicals in the mitochondria along with resident proteins are known to impact the conversion of hydroethidine and mitohydroethidine dyes to the red fluorescent bioproduct 2-hydroxyethidium. Furthermore, cytochrome C is known to interact with Mitosox Red dye, resulting in increased fluorescence.[80] Silica particles are known to increase cytochrome *c* levels, resulting in apoptosis.[42] Previously, we reported that another set of incinerated nanoclays induced apoptosis, albeit at much higher doses, in human bronchial epithelial cells.[21] Furthermore, it suggests cells potentially possessed adequate antioxidant defense mechanisms,[81] such as glutathione that showed a 40% reduction following 48 h Clois30B exposure in Caco2 cells.[53,69] Other studies, however, reported elevated intracellular ROS levels, but this is most likely to be dose-, bioassay method-, and nanoclay-dependent.[48,82,83]

Conversely, I-Clois30B and CS exposure was found to stimulate ROS production in NHLF cells, which did not correlate with cytotoxicity. Silica and quartz particles elevate ROS production in epithelial and fibroblasts via either inflammatory response, protein corona interaction, or surface reactivity,[84,85] which correlates with fibroblast stimulation and growth (KE5, Figure 7).[11,84,86,87] I-Clois30B, with crystalline structure more closely resembling CS than I-CloisNa, showed a similar response, possibly indicating that the crystal structure or surface reactivity may differentially impact lung fibroblast stimulation.[11,87] Unorganized surface silanol groups, including those on amorphous pyrogenic silica, are known to contribute to the transitory reactive nature of silica with cellular structures.[11] FTIR spectra comparison showed that I-Clois30B possessed a modest broad curve between 830 and 940 cm^{-1}, indicating Si−O−H which I-CloisNa did not possess.[19] All other spectra associated with silanol groups (3747−3000 cm^{-1}) were similar between incinerated nanoclays. In summary, pre-incinerated nanoclays differed from incinerated nanoclays in their MMP disruption and intracellular generation capacity, which potentially influenced cell viability, loss of membrane integrity (KE3), and inflammatory signaling (discussed below). Moreover, uncoated montmorillonite caused a depolarization of mitochondria, while the organic coating on ONC resulted in hyperpolarization that potentially impacts overall lung fibrotic response to montmorillonite exposure (KE5 and KE6).

Based on documented montmorillonite exposure capacity to induce DNA damage and observed changes in cell cycle shift in exposed cells that did completely align with changes in cell proliferation, we investigated nanoclay's capacity to induce micronuclei in SAECs. Clois30B, I-Clois30B, and CS exposure caused micronuclei in mononucleated cells, while cytokinesis block assay showed no change compared to unexposed controls. Increased micronuclei generation following Clois30B matches previous investigations.[48] Cloisite 30B and Clay 2 induced DNA damage in Comet assay and micronuclei, respectively, at similar noncytotoxic concentrations used in the present study.[44,69] In the present study, soluble QAC in cell culture medium released from Clois30B was not directly assessed but was potentially present.[73,74] Soluble coatings from the Clois30B particle and other QACs were shown to induce DNA damage via the Comet assay through a non-ROS-mediated unknown mechanism.[74,88,89] The high frequency of micronuclei at 20 μg/cm^2, however, is close to or above cytotoxic concentrations (∼51%); hence interpretation of micronuclei formation at this dose is limited due to the prevalence of other cytotoxic mechanisms producing nuclear fragments.[90] Our findings match those of previous studies showing that CloisNa and Clois30B do not induce micronuclei following a cytokinesis block at <20 μg/cm^2 (32 μg/mL);[58,91] however, higher doses can induce MN in vitro.[45] Some of the more cytotoxic quaternary ammonium compounds can cause micronucleus formation in exposed human and plant cells.[59,88] Next, incinerated nanoclay exposure at high doses causes elevated mitochondrial ROS, micronuclei, and subsequent cytotoxicity. Decan et al.[85] showed similar findings that single micron-sized amorphous silica induced ROS while micronuclei were reserved to nanosized silica in mouse lung epithelial cells. Micronuclei in mononucleated cells can arise from damaged cells that underwent DNA replication but no cell division, early in apoptosis, early in necrosis, or DNA strand breaks of cells in G_0.[92] The cell cycle shift to G_0/G_1 in Clois30B-exposed cells

https://doi.org/10.1021/acs.chemrestox.5c00206
Chem. Res. Toxicol. 2025, 38, 1708−1728

supports a potential cell cycle arrest to assess DNA damage and repair. Although not measured in this study, our previous and other investigations reported that ONCs, including those with QAC coatings, can induce 10−20% apoptosis in exposed epithelial cultures.[21,52] Given the reported in vitro and human worker ONC-induced DNA damage,[5] a more comprehensive study of nanoclay-induced genotoxicity and its potential adverse health outcomes following inhalation exposure remains understudied and an area for future research.

Next, only incinerated nanoclays and CS exposures produced elevated MCP-1, IL-6, and IL-8 levels in SAECs (KE1, Figure 7), which contrasted with pre-incinerated nanoclay exposures, significantly decreasing these pro-inflammatory cytokines. Several studies reported that amorphous silica exposure can produce several pro-inflammatory cytokines including IL-6, IL-8, and MCP-1.[93] IL-6 serves as a pro-inflammatory signal, initiates T_H2 differentiation, and can promote lung fibrosis,[94] while IL-8 and MCP-1 are neutrophil and macrophage recruitment signals.[95,96] Bentonite and ONC in vitro exposures can induce pro-inflammatory cytokine expression (e.g., IL-8)[22] but at higher and cytotoxic doses than tested in the present study. Several studies reported that nanosilica exposure, including nanoclay, decreases inflammatory cytokine expression (IL-6, TNFα) compared to controls in lung epithelial monoculture and coculture models,[69,97,98] while others report increases in pro-inflammatory cytokines.[93,99,100] It was not clear in this study what MIE was responsible for promoting an increased release of pro-inflammatory mediators (KE1). Factors including silica dose, size, morphology, surface area, crystal structure, and surface reactivity have been attributed to pro- and anti-inflammatory effects following exposure to mammalian lung epithelium. Our recent investigation found that human macrophages experienced a robust inflammatory response (including Il-1β, IL-8, and MCP-1) following pre-incinerated nanoclay exposure,[18] thus suggesting macrophages act as the primary lung inflammation initiators (KE1) for these particles. Conversely, both lung epithelial cells and macrophages play a pro-inflammatory role following incinerated nanoclay exposure.

Acute in vitro pre-incinerated nanoclay exposure caused NHLF activation (KE5) and pro-fibrotic potential evidenced by increased initial cell number, α-SMA expression, and collagen I expression, while incinerated nanoclay and CS caused less effect (Figure 7). Particle exposure in the deep lung can result in either direct or indirect activation of lung fibroblasts, resulting in a myofibroblast-like phenotype evidenced by their increased proliferation, TGFβ secretion, ROS, and α-SMA expression, which aids in wound repair and increased deposition of extracellular matrix and in pathological cases lead to lung fibrosis.[46−48] A majority of the nanoclay particles at ≤ 2 $\mu g/cm^2$ caused an increase in live NHLF counts after 24 h but did not enhance proliferation rate over 72 h compared to unexposed cells. To our knowledge, this is the second report of increased fibroblast cell number following direct nanoclay particulate exposure. Geh et al.[47] evaluated one ONC with different bentonite samples and reported elevated 6 to 19% proliferative capacity at 1 $\mu g/cm^2$ following 20 h of exposure, which coincides with this study. Biomedical polymer gels or tissue scaffolds containing nanoclay are increasingly used to stimulate fibroblast proliferation and promote wound healing.[101] Amorphous silica and aged CS can moderately stimulate cell proliferation and ROS at low to moderate doses,[87,102,103] which coincides with the present findings. Modest increases in Caspase 3/7 activity,[21] collagen I/III, α-SMA, and fibronectin expression with occasional proliferation stimulation confirms that incinerated nanoclay exposure possesses less inflammatory and pro-fibrotic effects than its pre-incinerated counterparts. Previous studies with CS reported enhanced fibroblast proliferation, while higher doses of raw or activated bentonite reported apoptosis, necrosis, and hemolytic effects.[82,87]

Several ENMs are known to directly interact with lung fibroblasts following exposure due to long biopersistence.[14,49] Previously, our in vivo study indicated a pro-fibrotic cytokine signature in C57BL/6 mouse lungs exposed to 300 μg of either CloisNa or Clois30B at Day 28 post-exposure.[16] Fibroblasts directly or indirectly exposed to particulate matter, including silica, can experience stimulation and activation of wound healing response characterized by proliferation, transition to myofibroblast phenotype (α-SMA), and secretion of extracellular matrices.[87,104,105] Direct silica exposure to fibroblasts was shown to (1) stimulate collagen production, but reduced TGFβ levels and inhibited TGFβ's stimulatory effect on ECM production[106] and (2) stimulate collagen and fibronectin synthesis in dermal fibroblast cells without inflammatory cell signals.[107] Although no solid evidence of direct in vivo nanoclay/fibroblast interaction data exists, it is plausible that rapid damage to epithelial monolayers by either CloisNa or Clois30B results in increased epithelial permeability and exposure of the interstitium to particulate matter (Figure 7). Increased PDGF-$\beta\beta$ secretion and correlation in both THP-1 in vitro and in vivo models at Day 7 postexposure suggests its potential role and importance in T_H2-mediated response, suppressing inflammation, enhancing fibrocyte chemotaxis, fibroblast proliferation, and pro-collagen I synthesis during wound healing or adverse pro-fibrotic response.[16,36,37,104,108,109]

In vitro exposure to pre- and post-incinerated nanoclays caused a robust collagen I response (KE6, Figure 7); however, this was not observed in vivo. Rather, in vitro collagen I expression correlated with in vivo soluble collagen I expression, irrespective of particle type, which coincides with earlier studies on carbon nanotubes and nano-CeO_2, showing good correlation of the in vitro/in vivo effect.[14,33] Mismatch between a strong in vitro and weak in vivo response possibly lies with differences in time course and the monoculture vs whole animal response. Soluble collagen I synthesis and deposition represent an early phase response in pulmonary fibrosis diseases typically associated with a wound healing response from activated fibroblasts and are observed in both in vitro and in vivo models. Other types of ECM deposition, including collagen III and reticular fibers, occurs during tissue remodeling stages that occur later in fibrotic pathogenesis that typically rely on immune and stromal cell crosstalk.[110−112] Nanometer thin platelets of montmorillonite, possessing silica oxide and aluminum oxide sheets, typically deposit deep in lung tissue and result in robust inflammation, granulomas, airway damage, poor clearance, and promotion of a silicosis-like pneumoconiosis disease characterized by excessive reticular fiber deposition.[9,113−115] Reticular fiber, usually comprised of collagen III, fibronectin, and other glycoproteins, under normal conditions, provides tissue flexibility and structure, while excessive deposition of reticular fiber and granulation tissue after damage results in scarring and occurs during middle stages of idiopathic fibrosis.[105,116,117] Reticular fiber deposition potentially relies on immune cell and resident

https://doi.org/10.1021/acs.chemrestox.5c00206
Chem. Res. Toxicol. 2025, 38, 1708−1728

stromal lung cell crosstalk, which was absent from our in vitro system. Additionally, the absence of a significant in vivo induction of ECM by either Clois30B or I-Clois30B suggests that the QAC coating reduces silica-associated promotion of ECM deposition. However, the presence of a pro-fibrotic BAL cytokine signature in Clois30B-exposed animals and indications of chronic inflammation similar to CS in I-Clois30B-exposed animals with biopersistent particulate suggests that the Day 28 time point potentially represents an early point in the development of a fibrotic-like disease and requires further investigation. Future mechanistic investigations using more complex co- or triculture models with appropriate immune cells could evaluate inflammatory cytokine and intercellular crosstalk time courses and ECM and reticular fiber synthesis dynamics following nanoclay exposures.

Previously, separate $nCeO_2$ and carbon nanotube exposures to primary NHLF produced a pro-fibrotic phenotype in vitro that correlated well with in vivo data.[14,33,118] TGF-β production by either resident macrophages or resident fibroblasts is established as a potent factor in stimulating lung fibroblast ECM and collagen production[119] and was found to undergo dose-dependent increased secretion in the above $nCeO_2$ and CNT studies. More recent investigations with CNTs with different morphologies[120] and the present study, however, reported that a nanomaterial's direct exposure to primary NHLF either did not produce a robust response or correlate with in vivo findings. For these two studies, increased TGF-β secretion was either minimal or nonexistent in either the cell culture model and/or in vivo studies.

The lack of clear agreement between responses of the monoculture SAEC and NHLF cultures and those observed in in vivo models following pre- and post-incinerated nanoclay exposure is most likely based on the absence of immune cell presence and crosstalk. Many of the adverse responses to nanoclay exposure observed in vivo rely on immune signaling and response.[16,23] Our recent in vitro study with these same particles with differentiated human macrophages aligned well with those immune effects observed in vivo.[18] Even though monoculture SAEC and NHLF models possess this shortcoming, they did supply further mechanistic information on several key events in these two cell types that promote adverse fibrotic responses. More complex co- and triculture air−liquid interface models with an immune cell component could help further investigate intercellular crosstalk and interactions, further assess single cell type's roles in adverse responses, and potentially result in better in vitro to in vivo concordance.

Several limitations in this study should be acknowledged. First no appropriate method exists to calculate the deposited dose of 2D particles in a submerged culture, which is largely dependent on particle size, morphology, medium characteristics, and ρ_{EV}. The delivered dose was not calculated in this study due to high uncertainty with stacking factor values (i.e., efficiency of agglomerate stacking) and low reliability of DLS analysis (Table S5) for 2D or high aspect ratio particles.[27,28,121] The uncertainty associated with ρ_{EV} with 2D materials is an area for further research. Second, it is unclear whether sonication procedures enhanced solubilization of QAC coatings into suspension preparations and eventually the cell culture medium. QAC coating solubilization can occur in cell culture medium suspensions[73,74] and potentially drive interactions with cell lipid membranes.[48,122] However, two different filtration studies with prepared ONC suspensions reported that a majority of the observed toxicity was due to intact ONC particles and not solubilized QAC coating.[17,52] Future studies should routinely conduct quantitative analytical analyses of ONC particle suspensions in cell culture medium and other physiological fluids to assess the role of QAC solubilization in driving toxicity. Third, the lack of clear in vitro vs in vivo agreement on nanoclay stimulation of ECM production is most likely due to several factors. No inflammatory cell presence or response signals were observed in our monoculture test system. ENMs are known to cause acute T_H1 inflammatory response followed by T_H2 anti-inflammatory/pro-fibrotic response, which is necessary for tissue damage recovery and remodeling that requires controlled deposition of the ECM matrix.[108,123] Dysregulated and/or prolonged T_H2 inflammatory response can prolong fibroblast stimulation, resulting in adverse lung fibrosis.[124] Without T_H1 or T_H2 (TGFβ, PDGF-$\beta\beta$) signaling present, several pro-fibrotic signaling mechanisms were most likely not activated. Moreover, several recent air−liquid interface studies using co- or tricultures with macrophages have shown that additional toxicity mechanisms occur between different cell types compared to monocultures.[125,126] Next, time differences of 48 h in vitro vs 28 days in vivo most likely impacted model agreement. Lastly, Western blot approaches are only able to detect soluble collagen protein at the time of sample collection and do not ascertain polymerized structural protein. Future nanoclay toxicity studies should evaluate more complex cultures to fully characterize intercellular signaling and extracellular matrix deposition to better understand KE within in vitro systems, thus improving in vitro to in vivo comparisons to assess lung fibrosis potential.

■ ASSOCIATED CONTENT

Data Availability Statement

The animal study protocol and procedures were approved by the NIOSH IACUC. A majority of the data generated or analyzed during this study are included in this published article [and its Supporting Information files]. Additional data sets used during the current study and the code block for generating ED_{50} curves are available from the corresponding author on reasonable request or can be found on the NIOSH Data and Statistics Gateway. The findings and conclusions in this article are those of the author(s) and do not necessarily represent the official position of the National Institute for Occupational Safety and Health, Centers for Disease Control and Prevention (CDC). Mention of any company or product does not constitute endorsement by NIOSH/CDC.

Supporting Information

The Supporting Information is available free of charge at https://pubs.acs.org/doi/10.1021/acs.chemrestox.5c00206.

Methods; results; staining methods for automated multiplex fluorescent imaging; particle hydrodynamic diameter and surface charge; particle characterization and secreted cytokine levels; and uptake, high-throughput imaging, and protein expression data (PDF)

■ AUTHOR INFORMATION

Corresponding Author

Todd A. Stueckle − *Health Effects Laboratory Division, National Institute for Occupational Safety and Health, Morgantown, West Virginia 26505, United States;*

https://doi.org/10.1021/acs.chemrestox.5c00206
Chem. Res. Toxicol. 2025, 38, 1708−1728

orcid.org/0000-0002-2495-7443; Phone: +1 (304) 285-6098; Email: jux5@cdc.gov

Authors

Jake Jensen − *Health Effects Laboratory Division, National Institute for Occupational Safety and Health, Morgantown, West Virginia 26505, United States*

Jayme P. Coyle − *Health Effects Laboratory Division, National Institute for Occupational Safety and Health, Morgantown, West Virginia 26505, United States*

Alixandra Wagner − *Chemical and Biomedical Engineering, West Virginia University, Morgantown, West Virginia 26506, United States*

Raymond Derk − *Health Effects Laboratory Division, National Institute for Occupational Safety and Health, Morgantown, West Virginia 26505, United States*

Tiffany G. Kornberg − *Health Effects Laboratory Division, National Institute for Occupational Safety and Health, Morgantown, West Virginia 26505, United States*

Sherri A. Friend − *Health Effects Laboratory Division, National Institute for Occupational Safety and Health, Morgantown, West Virginia 26505, United States*

Molly Schreiner − *Department of Public Health and Social Work, Slippery Rock University, Slippery Rock 16057, Pennsylvania*

Alexander C. Ufelle − *Department of Public Health and Social Work, Slippery Rock University, Slippery Rock 16057, Pennsylvania*

Sushant Agarwal − *Chemical and Biomedical Engineering, West Virginia University, Morgantown, West Virginia 26506, United States*

Rakesh K. Gupta − *Chemical and Biomedical Engineering, West Virginia University, Morgantown, West Virginia 26506, United States*

Cerasela Zoica Dinu − *Chemical and Biomedical Engineering, West Virginia University, Morgantown, West Virginia 26506, United States;* orcid.org/0000-0002-6474-6771

Liying W. Rojanasakul − *Health Effects Laboratory Division, National Institute for Occupational Safety and Health, Morgantown, West Virginia 26505, United States*

Complete contact information is available at: https://pubs.acs.org/10.1021/acs.chemrestox.5c00206

Author Contributions

The manuscript was written through contributions of all authors. All authors have given approval to the final version of the manuscript. TAS acquired funding, designed, carried out the study, and wrote the manuscript. JJ and JC designed and performed automated imaging studies and analyses. RD, TGK, and LR provided technical support, assisted animal work, and writing of the manuscript. SF performed all electron microscopy sample preparation and analysis. MS and ACU performed immunohistochemistry analysis. SA and RG provided nanoclay advice and assisted in drafting the manuscript. AW and CZD conducted XRD analysis and assisted in drafting the manuscript. CRediT: **Todd A Stueckle** conceptualization, data curation, formal analysis, funding acquisition, investigation, methodology, project administration, resources, supervision, visualization, writing - original draft, writing - review & editing; **Jake Jensen** data curation, formal analysis, investigation, methodology, writing - review & editing; **Jayme P Coyle** data curation, formal analysis, investigation, methodology, visualization, writing - original draft, writing - review & editing; **Raymond Derk** methodology, resources, writing - review & editing; **Tiffany G Kornberg** data curation, investigation, methodology, writing - review & editing; **Sherri A Friend** data curation, formal analysis, investigation, methodology, visualization, writing - review & editing; **Molly Schreiner** data curation, formal analysis, investigation, methodology, visualization, writing - review & editing; **Alexander C Ufelle** data curation, formal analysis, investigation, methodology, visualization, writing - original draft, writing - review & editing; **Sushant Agarwal** investigation, methodology, visualization, writing - review & editing; **Liying Rojanasakul** investigation, methodology, resources, supervision, writing - review & editing.

Funding

This study was supported by grants from the NIOSH Nanotechnology Research Center (939051L and 921043S), National Science Foundation Grant Nos. 1434503 and 1454230, the National Institutes of Health (ES022968), and a grant from the King Abdulaziz City for Science and Technology (Riyadh, Saudi Arabia).

Notes

The authors declare no competing financial interest.

■ ACKNOWLEDGMENTS

We thank the WVU Shared Research Facility and WVU Analytical Lab for their assistance with this study.

■ ABBREVIATIONS

AOP, Adverse outcome pathway; Cloisite Na^+, uncoated montmorillonite; Clois30B, Cloisite 30B, organomodified montmorillonite; I-CloisNa, Incinerated Cloisite Na^+; I-Clois30B, Incinerated Cloisite 30B; CS, Heat-inactivated crystalline silica; ELISA, enzyme-linked immunosorbent assay; FESEM, field emission scanning electron microscopy; HTS, high-throughput screening; KE, Key event; MIE, Molecular initiating event; MMP, mitochondrial membrane potential; NHLF, primary normal human lung fibroblast; ONC, organomodified nanoclay; QAC, quaternary ammonium compound; SAEC, small airway epithelial cells; TEM, transmission electron microscopy; THP-1, Human monocytic cells; XRD, X-ray diffraction

■ REFERENCES

(1) Arpita, K. Y. P. *Nanoclays Market by Product (Montmorillonite, Kaolinite, Smectite, Others), by Application (Water Treatment, Food and Beverage Packaging, Automotive, Biomedical, Paints and Coatings, Others). 2021−2031, 2022*; Global Opportunity Analysis and Industry Forecast, August, 2022.

(2) Analysts, G. I. *Global Nanoclay Industry. 2022* October 2022. Contract No.: 5961056.

(3) Mackevica, A.; Foss Hansen, S. Release of nanomaterials from solid nanocomposites and consumer exposure assessment - a forward-looking review. *Nanotoxicology* **2016**, *10* (6), 641−653.

(4) Zeng, S. L. Y. Z. Y.; Zhang, Q. F.; Du, Y. J.; Sun, Y. T.; Zhang, M. J. Study on occupational standard of bentonite dust in air of workplace. *Chin. J. Ind. Hyg. Occup. Dis.* **1998**, *16*, 177−178.

(5) Huang, Y.; Zhang, M.; Zou, H.; Li, X.; Xing, M.; Fang, X.; et al. Genetic damage and lipid peroxidation in workers occupationally exposed to organic bentonite particles. *Mutat. Res., Genet. Toxicol. Environ. Mutagen.* **2013**, *751* (1), 40−44.

(6) Holder, A. L.; Vejerano, E. P.; Zhou, X.; Marr, L. C. Nanomaterial disposal by incineration. *Environ. Sci.:Processes Impacts* **2013**, *15* (9), 1652−1664.

(7) Sotiriou, G. A.; Singh, D.; Zhang, F.; Chalbot, M. G.; Spielman-Sun, E.; Hoering, L.; et al. Thermal decomposition of nano-enabled thermoplastics: Possible environmental health and safety implications. *J. Hazard. Mater.* **2016**, *305*, 87−95.
(8) Timar, M.; Kendrey, G.; Juhasz, Z. Experimental observations concerning the effects of mineral dust to pulmonary tissue. *Med. Lav.* **1966**, *57* (1), 1−9.
(9) Ungváry, G.; Timár, M.; Tátrai, E.; Bácsy, E.; Gaál, G. Analysis of aluminium-silicate storage foci in the lungs. *Exp. Pathol.* **1983**, *23* (4), 203−214.
(10) Adamis, Z.; Williams, R. B. *Bentonite, Kaolin and Selected Clay Minerals*, 1st ed.; World Health Organization, 2005; p 191.
(11) Pavan, C.; Fubini, B. Unveiling the Variability of "Quartz Hazard" in Light of Recent Toxicological Findings. *Chem. Res. Toxicol.* **2017**, *30* (1), 469−485.
(12) Halappanavar, S. S. M., Wallin, H., Vogel, U., Sullivan, K., Clippinger, A. J. AOP 173: Substance interaction with the lung resident cell membrane components leading to lung fibrosis 2023 [Available from: https://aopwiki.org/aops/173.]
(13) Mishra, A.; Stueckle, T. A.; Mercer, R. R.; Derk, R.; Rojanasakul, Y.; Castranova, V.; et al. Identification of TGF-β receptor-1 as a key regulator of carbon nanotube-induced fibrogenesis. *Am. J. Physiol Lung Cell Mol. Physiol* **2015**, *309* (8), L821−L833.
(14) Davidson, D. C.; Derk, R.; He, X.; Stueckle, T. A.; Cohen, J.; Pirela, S. V.; Demokritou, P.; Rojanasakul, Y.; Wang, L. Direct stimulation of human fibroblasts by nCeO2 in vitro is attenuated with an amorphous silica coating. *Part. Fibre Toxicol.* **2016**, *13* (1), 23.
(15) Ma, J. Y.; Mercer, R. R.; Barger, M.; Schwegler-Berry, D.; Scabilloni, J.; Ma, J. K.; et al. Induction of pulmonary fibrosis by cerium oxide nanoparticles. *Toxicol. Appl. Pharmacol.* **2012**, *262* (3), 255−264.
(16) Stueckle, T. A.; Davidson, D. C.; Derk, R.; Kornberg, T. G.; Battelli, L.; Friend, S.; et al. Short-Term Pulmonary Toxicity Assessment of Pre- and Post-incinerated Organomodified Nanoclay in Mice. *ACS Nano* **2018**, *12* (3), 2292−2310.
(17) Di Ianni, E.; Møller, P.; Mortensen, A.; Szarek, J.; Clausen, P. A.; Saber, A. T.; et al. Organomodified nanoclays induce less inflammation, acute phase response, and genotoxicity than pristine nanoclays in mice lungs. *Nanotoxicology* **2020**, *14*, 869.
(18) Stueckle, T. A.; Jensen, J.; Coyle, J. P.; Derk, R.; Wagner, A.; Dinu, C. Z.; Kornberg, T. G.; Friend, S. A.; Dozier, A.; Agarwal, S.; et al. In vitro inflammation and toxicity assessment of pre- and post-incinerated organomodified nanoclays to macrophages using high-throughput screening approaches. *Part. Fibre Toxicol.* **2024**, *21* (1), 16.
(19) Wagner, A.; Eldawud, R.; White, A.; Agarwal, S.; Stueckle, T. A.; Sierros, K. A.; Rojanasakul, Y.; Gupta, R. K.; Dinu, C. Z. Toxicity evaluations of nanoclays and thermally degraded byproducts through spectroscopical and microscopical approaches. *Biochim. Biophys. Acta, Gen. Subj.* **2017**, *1861* (1), 3406−3415.
(20) Wagner, A.; White, A. P.; Stueckle, T. A.; Banerjee, D.; Sierros, K. A.; Rojanasakul, Y.; et al. Early Assessment and Correlations of Nanoclay's Toxicity to Their Physical and Chemical Properties. *ACS Appl. Mater. Interfaces* **2017**, *9* (37), 32323−32335.
(21) Stueckle, T. A.; White, A.; Wagner, A.; Gupta, R. K.; Rojanasakul, Y.; Dinu, C. Z. Impacts of Organomodified Nanoclays and Their Incinerated Byproducts on Bronchial Cell Monolayer Integrity. *Chem. Res. Toxicol.* **2019**, *32* (12), 2445−2458.
(22) Di Ianni, E.; Møller, P.; Vogel, U. B.; Jacobsen, N. R. Pro-inflammatory response and genotoxicity caused by clay and graphene nanomaterials in A549 and THP-1 cells. *Mutat. Res., Genet. Toxicol. Environ. Mutagen.* **2021**, *872*, 503405.
(23) Stueckle, T. A. C. J., Shane, H., Orandle, M. S., Jensen, J., Roach, K., Johnson, C., Derk, R., Battelli, L., Richardson, D., Friend, S., Gupta, R. K., Dinu, C. Z., Lee, E.; Rojanasakul, L. Histopathological and inflammatory indices comparison of mouse lung following repeat exposure to nanoclay and machined nanoclay composite dusts. In *61st Annual Society of Toxicology Meeting and ToxExpo*; Toxicological Sciences: San Diego, CA, USA, 2022, 5030.
(24) Porter, D. W.; Barger, M.; Robinson, V. A.; Leonard, S. S.; Landsittel, D.; Castranova, V. Comparison of low doses of aged and freshly fractured silica on pulmonary inflammation and damage in the rat. *Toxicology* **2002**, *175* (1−3), 63−71.
(25) Cohen, J. M.; Beltran-Huarac, J.; Pyrgiotakis, G.; Demokritou, P. Effective delivery of sonication energy to fast settling and agglomerating nanomaterial suspensions for cellular studies: Implications for stability, particle kinetics, dosimetry and toxicity. *NanoImpact* **2018**, *10*, 81−86.
(26) Coyle, J. P.; Derk, R. C.; Kornberg, T. G.; Singh, D.; Jensen, J.; Friend, S.; Mercer, R.; Stueckle, T. A.; Demokritou, P.; Rojanasakul, Y.; et al. Carbon nanotube filler enhances incinerated thermoplastics-induced cytotoxicity and metabolic disruption in vitro. *Part. Fibre Toxicol.* **2020**, *17*, 40.
(27) DeLoid, G.; Cohen, J. M.; Darrah, T.; Derk, R.; Rojanasakul, L.; Pyrgiotakis, G.; et al. Estimating the effective density of engineered nanomaterials for in vitro dosimetry. *Nat. Commun.* **2014**, *5*, 3514.
(28) Yue, Y.; Kan, Y.; Choi, H.; Clearfield, A.; Liang, H. J. A. P. L. Correlating hydrodynamic radii with that of two-dimensional nanoparticles. *Appl. Phys. Lett.* **2015**, *107* (25), 253103.
(29) Stueckle, T. A.; Davidson, D. C.; Derk, R.; Kornberg, T. G.; Schwegler-Berry, D.; Pirela, S. V.; et al. Evaluation of tumorigenic potential of CeO2 and Fe2O3 engineered nanoparticles by a human cell in vitro screening model. *NanoImpact* **2017**, *6*, 39−54.
(30) Piao, C. Q.; Liu, L.; Zhao, Y. L.; Balajee, A. S.; Suzuki, M.; Hei, T. K. Immortalization of human small airway epithelial cells by ectopic expression of telomerase. *Carcinogenesis* **2005**, *26* (4), 725−731.
(31) Wang, L.; Stueckle, T. A.; Mishra, A.; Derk, R.; Meighan, T.; Castranova, V.; et al. Neoplastic-like transformation effect of single-walled and multi-walled carbon nanotubes compared to asbestos on human lung small airway epithelial cells. *Nanotoxicology* **2014**, *8* (5), 485−507.
(32) Hiemstra, P. S.; Grootaers, G.; Kooter, I. M.; van der Does, A. M.; Krul, C. A. M. Human lung epithelial cell cultures for analysis of inhaled toxicants: Lessons learned and future directions. *Toxicol. In Vitro* **2018**, *47*, 137.
(33) Wang, L.; Mercer, R. R.; Rojanasakul, Y.; Qiu, A.; Lu, Y.; Scabilloni, J. F.; et al. Direct fibrogenic effects of dispersed single-walled carbon nanotubes on human lung fibroblasts. *J. Toxicol. Environ. Health, Part A* **2010**, *73* (5), 410−422.
(34) Hubbs, A.; Greskevitch, M.; Kuempel, E.; Suarez, F.; Toraason, M. Abrasive blasting agents: designing studies to evaluate relative risk. *J. Toxicol. Environ. Health, Part A* **2005**, *68* (11−12), 999−1016.
(35) Coyle, J. P.; Johnson, C.; Jensen, J.; Farcas, M.; Derk, R.; Stueckle, T. A.; Kornberg, T. G.; Rojanasakul, Y.; Rojanasakul, L. W. Variation in pentose phosphate pathway-associated metabolism dictates cytotoxicity outcomes determined by tetrazolium reduction assays. *Sci. Rep.* **2023**, *13* (1), 8220.
(36) Aono, Y.; Kishi, M.; Yokota, Y.; Azuma, M.; Kinoshita, K.; Takezaki, A.; et al. Role of platelet-derived growth factor/platelet-derived growth factor receptor axis in the trafficking of circulating fibrocytes in pulmonary fibrosis. *Am. J. Respir. Cell Mol. Biol.* **2014**, *51* (6), 793−801.
(37) Distler, J. H. W.; Györfi, A. H.; Ramanujam, M.; Whitfield, M. L.; Königshoff, M.; Lafyatis, R. Shared and distinct mechanisms of fibrosis. *Nat. Rev. Rheumatol.* **2019**, *15* (12), 705−730.
(38) Antar, S. A.; Ashour, N. A.; Marawan, M. E.; Al-Karmalawy, A. A. Fibrosis: Types, Effects, Markers, Mechanisms for Disease Progression, and Its Relation with Oxidative Stress, Immunity, and Inflammation. *Int. J. Mol. Sci.* **2023**, *24* (4), 4004.
(39) Stone, K. C.; Mercer, R. R.; Freeman, B. A.; Chang, L. Y.; Crapo, J. D. Distribution of lung cell numbers and volumes between alveolar and nonalveolar tissue. *Am. Rev. Respir. Dis.* **1992**, *146* (2), 454−456.
(40) Latoche, J. D.; Ufelle, A. C.; Fazzi, F.; Ganguly, K.; Leikauf, G. D.; Fattman, C. L. Secreted Phosphoprotein 1 and Sex-Specific

https://doi.org/10.1021/acs.chemrestox.5c00206
Chem. Res. Toxicol. 2025, 38, 1708−1728

Differences in Silica-Induced Pulmonary Fibrosis in Mice. *Environ. Health Perspect.* **2016**, *124* (8), 1199−1207.
(41) Guo, C.; Wang, J.; Jing, L.; Ma, R.; Liu, X.; Gao, L.; et al. Mitochondrial dysfunction, perturbations of mitochondrial dynamics and biogenesis involved in endothelial injury induced by silica nanoparticles. *Environ. Pollut.* **2018**, *236*, 926−936.
(42) Sun, L.; Li, Y.; Liu, X.; Jin, M.; Zhang, L.; Du, Z.; et al. Cytotoxicity and mitochondrial damage caused by silica nanoparticles. *Toxicol. In Vitro* **2011**, *25* (8), 1619−1629.
(43) Suski, J.; Lebiedzinska, M.; Bonora, M.; Pinton, P.; Duszynski, J.; Wieckowski, M. R. Relation Between Mitochondrial Membrane Potential and ROS Formation. *Methods Mol. Biol.* **2018**, *1782*, 357−381.
(44) Maisanaba, S.; Hercog, K.; Ortuno, N.; Jos, A.; Zegura, B. Induction of micronuclei and alteration of gene expression by an organomodified clay in HepG2 cells. *Chemosphere* **2016**, *154*, 240−248.
(45) Maisanaba, S.; Hercog, K.; Filipic, M.; Jos, A.; Zegura, B. Genotoxic potential of montmorillonite clay mineral and alteration in the expression of genes involved in toxicity mechanisms in the human hepatoma cell line HepG2. *J. Hazard. Mater.* **2016**, *304*, 425−433.
(46) Tatrai, E.; Adamis, Z.; Timar, M.; Unkváry, G. Comparative histopathological and biochemical analysis of early stages of exposure to non-silicogenic aluminium silicate- and strongly silicogenic quartz-dust in rats. *Exp. Pathol.* **1983**, *23* (3), 163−171.
(47) Geh, S.; Yücel, R.; Duffin, R.; Albrecht, C.; Borm, P. J.; Armbruster, L.; et al. Cellular uptake and cytotoxic potential of respirable bentonite particles with different quartz contents and chemical modifications in human lung fibroblasts. *Arch. Toxicol.* **2006**, *80* (2), 98−106.
(48) Maisanaba, S.; Pichardo, S.; Puerto, M.; Gutierrez-Praena, D.; Camean, A. M.; Jos, A. Toxicological evaluation of clay minerals and derived nanocomposites: a review. *Environ. Res.* **2015**, *138*, 233−254.
(49) Kumar, C.; Srivastava, S. Structural and Dynamical Studies of a Lipid-Nanoclay Composite Layer at the Air-Water Interface. *Langmuir* **2022**, *38* (34), 10400−10411.
(50) Kondej, D.; Sosnowski, T. R. Effect of clay nanoparticles on model lung surfactant: a potential marker of hazard from nanoaerosol inhalation. *Environ. Sci. Pollut Res. Int.* **2016**, *23* (5), 4660−4669.
(51) Kondej, D.; Sosnowski, T. R. Alteration of biophysical activity of pulmonary surfactant by aluminosilicate nanoparticles. *Inhalation Toxicol.* **2013**, *25* (2), 77−83.
(52) Janer, G.; Fernandez-Rosas, E.; Mas del Molino, E.; Gonzalez-Galvez, D.; Vilar, G.; Lopez-Iglesias, C.; et al. In vitro toxicity of functionalised nanoclays is mainly driven by the presence of organic modifiers. *Nanotoxicology* **2014**, *8* (3), 279−294.
(53) Maisanaba, S.; Gutierrez-Praena, D.; Pichardo, S.; Moreno, F. J.; Jorda, M.; Camean, A. M.; et al. Toxic effects of a modified montmorillonite clay on the human intestinal cell line Caco-2. *J. Appl. Toxicol.* **2014**, *34* (6), 714−725.
(54) Beliveau, A.; Yaswen, P. Soothing the watchman: telomerase reduces the p53-dependent cellular stress response. *Cell Cycle* **2007**, *6* (11), 1284−1287.
(55) Sabzevari, A. G.; Sabahi, H.; Nikbakht, M. Montmorillonite, a natural biocompatible nanosheet with intrinsic antitumor activity. *Colloids Surf., B* **2020**, *190*, 110884.
(56) Murugadoss, S.; Lison, D.; Godderis, L.; Van Den Brule, S.; Mast, J.; Brassinne, F.; et al. Toxicology of silica nanoparticles: an update. *Arch. Toxicol.* **2017**, *91* (9), 2967−3010.
(57) Gonzalez, L.; Lukamowicz-Rajska, M.; Thomassen, L. C.; Kirschhock, C. E.; Leyns, L.; Lison, D.; et al. Co-assessment of cell cycle and micronucleus frequencies demonstrates the influence of serum on the in vitro genotoxic response to amorphous monodisperse silica nanoparticles of varying sizes. *Nanotoxicology* **2014**, *8* (8), 876−884.
(58) Maser, E.; Schulz, M.; Sauer, U. G.; Wiemann, M.; Ma-Hock, L.; Wohlleben, W.; et al. In vitro and in vivo genotoxicity investigations of differently sized amorphous SiO2 nanomaterials. *Mutat Res. Genet Toxicol Environ. Mutagen.* **2015**, *794*, 57−74.
(59) Borm, P. J. A.; Fowler, P.; Kirkland, D. An updated review of the genotoxicity of respirable crystalline silica. *Part. Fibre Toxicol.* **2018**, *15* (1), 23.
(60) Brandão, F.; Costa, C.; Bessa, M. J.; Valdiglesias, V.; Hellack, B.; Haase, A.; et al. Multiparametric in vitro genotoxicity assessment of different variants of amorphous silica nanomaterials in rat alveolar epithelial cells. *Nanotoxicology* **2023**, *17* (6−7), 511−528.
(61) Wagner, A.; White, A. P.; Tang, M. C.; Agarwal, S.; Stueckle, T. A.; Rojanasakul, Y.; Gupta, R. K.; Dinu, C. Z. Incineration of Nanoclay Composites Leads to Byproducts with Reduced Cellular Reactivity. *Sci. Rep.* **2018**, *8* (1), 10709.
(62) Wang, Y.; Nartiss, Y.; Steipe, B.; McQuibban, G. A.; Kim, P. K. ROS-induced mitochondrial depolarization initiates PARK2/PARKIN-dependent mitochondrial degradation by autophagy. *Autophagy* **2012**, *8* (10), 1462−1476.
(63) Marrocco, A.; Ortiz, L. A. Role of metabolic reprogramming in pro-inflammatory cytokine secretion from LPS or silica-activated macrophages. *Front. Immunol.* **2022**, *13*, 936167.
(64) Joshi, G. N.; Goetjen, A. M.; Knecht, D. A. Silica particles cause NADPH oxidase-independent ROS generation and transient phagolysosomal leakage. *Mol. Biol. Cell* **2015**, *26* (18), 3150−3164.
(65) Joshi, G. N.; Knecht, D. A. Silica phagocytosis causes apoptosis and necrosis by different temporal and molecular pathways in alveolar macrophages. *Apoptosis* **2013**, *18* (3), 271−285.
(66) Sack, M. N. Mitochondrial depolarization and the role of uncoupling proteins in ischemia tolerance. *Cardiovasc. Res.* **2006**, *72* (2), 210−219.
(67) Li, S.; Cortez-Jugo, C.; Ju, Y.; Caruso, F. Approaching Two Decades: Biomolecular Coronas and Bio-Nano Interactions. *ACS Nano* **2024**, *18* (49), 33257−33263.
(68) Lanone, S.; Rogerieux, F.; Geys, J.; Dupont, A.; Maillot-Marechal, E.; Boczkowski, J.; et al. Comparative toxicity of 24 manufactured nanoparticles in human alveolar epithelial and macrophage cell lines. *Part. Fibre Toxicol.* **2009**, *6*, 14.
(69) Maisanaba, S.; Puerto, M.; Pichardo, S.; Jorda, M.; Moreno, F. J.; Aucejo, S.; et al. In vitro toxicological assessment of clays for their use in food packaging applications. *Food Chem. Toxicol.* **2013**, *57*, 266−275.
(70) Inácio, A. S.; Costa, G. N.; Domingues, N. S.; Santos, M. S.; Moreno, A. J. M.; Vaz, W. L. C.; et al. Mitochondrial dysfunction is the focus of quaternary ammonium surfactant toxicity to mammalian epithelial cells. *Antimicrob. Agents Chemother.* **2013**, *57* (6), 2631−2639.
(71) Inacio, A. S.; Domingues, N. S.; Nunes, A.; Martins, P. T.; Moreno, M. J.; Estronca, L. M.; et al. Quaternary ammonium surfactant structure determines selective toxicity towards bacteria: mechanisms of action and clinical implications in antibacterial prophylaxis. *J. Antimicrob. Chemother.* **2016**, *71* (3), 641−654.
(72) Rogov, A. G.; Goleva, T. N.; Sukhanova, E. I.; Epremyan, K. K.; Trendeleva, T. A.; Ovchenkova, A. P.; Aliverdieva, D. A.; Zvyagilskaya, R. A. Mitochondrial Dysfunctions May Be One of the Major Causative Factors Underlying Detrimental Effects of Benzalkonium Chloride. *Oxid. Med. Cell. Longevity* **2020**, *2020*, 1−14.
(73) Sharma, A. K.; Mortensen, A.; Schmidt, B.; Frandsen, H.; Hadrup, N.; Larsen, E. H.; et al. In-vivo study of genotoxic and inflammatory effects of the organo-modified Montmorillonite Cloisite(R) 30B. *Mutat Res. Genet Toxicol Environ. Mutagen.* **2014**, *770*, 66−71.
(74) Sharma, A. K.; Schmidt, B.; Frandsen, H.; Jacobsen, N. R.; Larsen, E. H.; Binderup, M. L. Genotoxicity of unmodified and organo-modified montmorillonite. *Mutat. Res.* **2010**, *700* (1−2), 18−25.
(75) Won, J.-H.; Park, S.; Hong, S.; Son, S.; Yu, J.-W. J. JoB. C. Rotenone-induced impairment of mitochondrial electron transport chain confers a selective priming signal for NLRP3 inflammasome activation. *J. Biol. Chem.* **2015**, *290* (45), 27425−27437.
(76) Perl, A.; Gergely, P., Jr.; Nagy, G.; Koncz, A.; Banki, K. Mitochondrial hyperpolarization: a checkpoint of T-cell life, death and autoimmunity. *Trends Immunol.* **2004**, *25* (7), 360−367.

https://doi.org/10.1021/acs.chemrestox.5c00206
Chem. Res. Toxicol. 2025, 38, 1708−1728

(77) Deville, S.; Honrath, B.; Tran, Q. T. D.; Fejer, G.; Lambrichts, I.; Nelissen, I.; et al. Time-resolved characterization of the mechanisms of toxicity induced by silica and amino-modified polystyrene on alveolar-like macrophages. *Arch. Toxicol.* **2020**, *94* (1), 173−186.
(78) Zhang, H.; Dunphy, D. R.; Jiang, X.; Meng, H.; Sun, B.; Tarn, D.; et al. Processing pathway dependence of amorphous silica nanoparticle toxicity: colloidal vs pyrolytic. *J. Am. Chem. Soc.* **2012**, *134* (38), 15790−15804.
(79) Rubio, L.; Pyrgiotakis, G.; Beltran-Huarac, J.; Zhang, Y.; Gaurav, J.; Deloid, G.; Spyrogianni, A.; Sarosiek, K. A.; Bello, D.; Demokritou, P. Safer-by-design flame-sprayed silicon dioxide nanoparticles: the role of silanol content on ROS generation, surface activity and cytotoxicity. *Part. Fibre Toxicol.* **2019**, *16* (1), 40.
(80) Zielonka, J.; Kalyanaraman, B. Hydroethidine- and MitoSOX-derived red fluorescence is not a reliable indicator of intracellular superoxide formation: another inconvenient truth. *Free Radic Biol. Med.* **2010**, *48* (8), 983−1001.
(81) Dikalov, S. I.; Harrison, D. G. Methods for detection of mitochondrial and cellular reactive oxygen species. *Antioxid Redox Signal* **2014**, *20* (2), 372−382.
(82) Baek, M.; Lee, J.-A.; Choi, S.-J. Toxicological effects of a cationic clay, montmorillonite in vitro and in vivo. *Mol. Cell. Toxicol.* **2012**, *8* (1), 95−101.
(83) Ruijter, N.; van der Zee, M.; Katsumiti, A.; Boyles, M.; Cassee, F. R.; Braakhuis, H. Improving the dichloro-dihydro-fluorescein (DCFH) assay for the assessment of intracellular reactive oxygen species formation by nanomaterials. *NanoImpact* **2024**, *35*, 100521.
(84) Li, Y.; Wang, P.; Hu, C.; Wang, K.; Chang, Q.; Liu, L.; Han, Z.; Shao, Y.; Zhai, Y.; Zuo, Z.; et al. Protein corona of airborne nanoscale PM2.5 induces aberrant proliferation of human lung fibroblasts based on a 3D organotypic culture. *Sci. Rep.* **2018**, *8* (1), 1939.
(85) Decan, N.; Wu, D.; Williams, A.; Bernatchez, S.; Johnston, M.; Hill, M.; et al. Characterization of in vitro genotoxic, cytotoxic and transcriptomic responses following exposures to amorphous silica of different sizes. *Mutat. Res., Genet. Toxicol. Environ. Mutagen.* **2016**, *796*, 8−22.
(86) Driscoll, K. E. The toxicology of crystalline silica studied in vitro. *Appl. Occup. Environ. Hyg.* **1995**, *10* (12), 1118.
(87) Pozzolini, M.; Vergani, L.; Ragazzoni, M.; Delpiano, L.; Grasselli, E.; Voci, A.; et al. Different reactivity of primary fibroblasts and endothelial cells towards crystalline silica: A surface radical matter. *Toxicology* **2016**, *361*−*362*, 12−23.
(88) Ferk, F.; Misík, M.; Hoelzl, C.; Uhl, M.; Fuerhacker, M.; Grillitsch, B.; et al. Benzalkonium chloride (BAC) and dimethyldioctadecyl-ammonium bromide (DDAB), two common quaternary ammonium compounds, cause genotoxic effects in mammalian and plant cells at environmentally relevant concentrations. *Mutagenesis* **2007**, *22* (6), 363−370.
(89) Deutschle, T.; Porkert, U.; Reiter, R.; Keck, T.; Riechelmann, H. In vitro genotoxicity and cytotoxicity of benzalkonium chloride. *Toxicol. In Vitro* **2006**, *20* (8), 1472−1477.
(90) OECD *In Vitro Mammalian Chromosome Aberration Test*, 2014.
(91) Maisanaba, S.; Jordá-Beneyto, M.; Cameán, A. M.; Jos, A. Effects of two organomodified clays intended to food contact materials on the genomic instability and gene expression of hepatoma cells. *Food Chem. Toxicol.* **2016**, *88*, 57−64.
(92) Kirsch-Volders, M.; Fenech, M. Inclusion of micronuclei in non-divided mononuclear lymphocytes and necrosis/apoptosis may provide a more comprehensive cytokinesis block micronucleus assay for biomonitoring purposes. *Mutagenesis* **2001**, *16* (1), 51−58.
(93) Marques Da Silva, V.; Benjdir, M.; Montagne, P.; Pairon, J. C.; Lanone, S.; Andujar, P. Pulmonary Toxicity of Silica Linked to Its Micro- or Nanometric Particle Size and Crystal Structure: A Review. *Nanomaterials* **2022**, *12* (14), 2392.
(94) Le, T. T.; Karmouty-Quintana, H.; Melicoff, E.; Le, T. T.; Weng, T.; Chen, N. Y.; et al. Blockade of IL-6 Trans signaling attenuates pulmonary fibrosis. *J. Immunol.* **2014**, *193* (7), 3755−3768.
(95) Cross, L. J.; Matthay, M. A. Biomarkers in acute lung injury: insights into the pathogenesis of acute lung injury. *Crit. Care Clin.* **2011**, *27* (2), 355−377.
(96) Kawasaki, H. A mechanistic review of silica-induced inhalation toxicity. *Inhalation Toxicol.* **2015**, *27* (8), 363−377.
(97) Hofmann, F.; Bläsche, R.; Kasper, M.; Barth, K. A co-culture system with an organotypic lung slice and an immortal alveolar macrophage cell line to quantify silica-induced inflammation. *PLoS One* **2015**, *10* (1), No. e0117056.
(98) J, H.; D, M.; M, P.; D, G.-P.; M, J.; S, A.; A, J. Toxicity assessment of organomodified clays used in food contact materials on human target cell lines. *Appl. Clay Sci.* **2014**, *90*, 150.
(99) Skuland, T.; Ovrevik, J.; Låg, M.; Schwarze, P.; Refsnes, M. Silica nanoparticles induce cytokine responses in lung epithelial cells through activation of a p38/TACE/TGF-α/EGFR-pathway and NF-κB signalling. *Toxicol. Appl. Pharmacol.* **2014**, *279* (1), 76−86.
(100) Skuland, T.; Låg, M.; Gutleb, A. C.; Brinchmann, B. C.; Serchi, T.; Øvrevik, J.; Holme, J. A.; Refsnes, M. Pro-inflammatory effects of crystalline- and nano-sized non-crystalline silica particles in a 3D alveolar model. *Part. Fibre Toxicol.* **2020**, *17* (1), 13.
(101) Miele, D.; Ruggeri, M.; Vigani, B.; Viseras, C.; Natali, F.; Del Favero, E.; et al. Nanoclay-Doped Electrospun Nanofibers for Tissue Engineering: Investigation on the Structural Modifications in Physiological Environment. *Int. J. Nanomed.* **2023**, *18*, 7695−7710.
(102) Wittig, A.; Gehrke, H.; Del Favero, G.; Fritz, E.-M.; Al-Rawi, M.; Diabaté, S.; et al. Amorphous silica particles relevant in food industry influence cellular growth and associated signaling pathways in human gastric carcinoma cells. *Nanomaterials* **2017**, *7* (1), 18.
(103) Kim, K. J.; Joe, Y. A.; Kim, M. K.; Lee, S. J.; Ryu, Y. H.; Cho, D. W.; et al. Silica nanoparticles increase human adipose tissue-derived stem cell proliferation through ERK1/2 activation. *Int. J. Nanomed.* **2015**, *10*, 2261−2272.
(104) Lewis, C. C.; Chu, H. W.; Westcott, J. Y.; Tucker, A.; Langmack, E. L.; Sutherland, E. R.; Kraft, M. Airway fibroblasts exhibit a synthetic phenotype in severe asthma. *J. Allergy Clin. Immunol.* **2005**, *115* (3), 534−540.
(105) Kalluri, R. The biology and function of fibroblasts in cancer. *Nat. Rev. Cancer* **2016**, *16* (9), 582−598.
(106) Baroni, T.; Bodo, M.; D'Alessandro, A.; Conte, C.; Calvitti, M.; Muzi, G.; et al. Silica and its antagonistic effects on transforming growth factor-β in lung fibroblast extracellular matrix production. *J. Invest. Med.* **2001**, *49* (2), 146−156.
(107) Li, Y.; Kilani, R. T.; Hartwell, R.; Ghahary, A. MAP kinase mediates silica-induced fibrotic nodule formation and collagen accumulation in fibroblasts. *J. Cell. Physiol.* **2012**, *227* (1), 328−338.
(108) Dong, J.; Ma, Q. Type 2 Immune Mechanisms in Carbon Nanotube-Induced Lung Fibrosis. *Front. Immunol.* **2018**, *9*, 1120.
(109) Wang, X.; Sun, B.; Liu, S.; Xia, T. Structure Activity Relationships of Engineered Nanomaterials in inducing NLRP3 Inflammasome Activation and Chronic Lung Fibrosis. *NanoImpact* **2017**, *6*, 99−108.
(110) Herrera, J.; Henke, C. A.; Bitterman, P. B. Extracellular matrix as a driver of progressive fibrosis. *J. Clin. Invest.* **2018**, *128* (1), 45−53.
(111) Savin, I. A.; Zenkova, M. A.; Sen'kova, A. V. Pulmonary Fibrosis as a Result of Acute Lung Inflammation: Molecular Mechanisms, Relevant In Vivo Models, Prognostic and Therapeutic Approaches. *Int. J. Mol. Sci.* **2022**, *23* (23), 14959.
(112) Júnior, C.; Ulldemolins, A.; Narciso, M.; Almendros, I.; Farré, R.; Navajas, D.; López, J.; Eroles, M.; Rico, F.; Gavara, N. Multi-Step Extracellular Matrix Remodelling and Stiffening in the Development of Idiopathic Pulmonary Fibrosis. *Int. J. Mol. Sci.* **2023**, *24* (2), 1708.
(113) Schreider, J. P.; Culbertson, M. R.; Raabe, O. G. Comparative pulmonary fibrogenic potential of selected particles. *Environ. Res.* **1985**, *38* (2), 256−274.
(114) Gibbs, A. R.; Pooley, F. D. Fuller's earth (montmorillonite) pneumoconiosis. *Occup. Environ. Med.* **1994**, *51* (9), 644−646.
(115) Sakula, A. J. T. Pneumoconiosis due to fuller. *s earth* **1961**, *16* (2), 176.

https://doi.org/10.1021/acs.chemrestox.5c00206
Chem. Res. Toxicol. 2025, 38, 1708−1728

(116) Djeska, I. S.; Ceausu, R. A.; Gaje, P. N.; Cimpean, A. M.; Mederle, O.; Nicodin, A.; Tudorache, V.; Raica, M. The reticular network contributes to the staging of idiopathic lung fibrosis. *Arch. Biol. Sci.* **2013**, *65* (4), 1599−1604.
(117) Darby, I. A.; Laverdet, B.; Bonté, F.; Desmoulière, A. Fibroblasts and myofibroblasts in wound healing. *Clin., Cosmet. Invest. Dermatol.* **2014**, *7*, 301−311.
(118) Manke, A.; Luanpitpong, S.; Dong, C.; Wang, L.; He, X.; Battelli, L.; et al. Effect of fiber length on carbon nanotube-induced fibrogenesis. *Int. J. Mol. Sci.* **2014**, *15* (5), 7444−7461.
(119) Agostini, C.; Gurrieri, C. Chemokine/cytokine cocktail in idiopathic pulmonary fibrosis. *Proc. Am. Thorac Soc.* **2006**, *3* (4), 357−363.
(120) Fraser, K.; Hubbs, A.; Yanamala, N.; Mercer, R. R.; Stueckle, T. A.; Jensen, J.; Eye, T.; Battelli, L.; Clingerman, S.; Fluharty, K.; et al. Histopathology of the broad class of carbon nanotubes and nanofibers used or produced in U.S. facilities in a murine model. *Part. Fibre Toxicol.* **2021**, *18* (1), 47.
(121) Cohen, J. M.; Teeguarden, J. G.; Demokritou, P. An integrated approach for the in vitro dosimetry of engineered nanomaterials. *Part. Fibre Toxicol.* **2014**, *11*, 20.
(122) Simberg, D.; Weisman, S.; Talmon, Y.; Barenholz, Y. DOTAP (and other cationic lipids): chemistry, biophysics, and transfection. *Crit. Rev. Ther. Drug Carrier Syst.* **2004**, *21* (4), 257−317.
(123) Mishra, V.; Baranwal, V.; Mugale, M. N.; Sharma, S.; Mishra, R. K. Stat3 Induces IL-10 and SR-A/CD204 Expression in Silica Nanoparticle-Triggered Pulmonary Fibrosis through Transactivation. *ACS Biomater. Sci. Eng.* **2025**, *11* (1), 609−622.
(124) Spagnolo, P.; Tonelli, R.; Samarelli, A. V.; Castelli, G.; Cocconcelli, E.; Petrarulo, S.; et al. The role of immune response in the pathogenesis of idiopathic pulmonary fibrosis: far beyond the Th1/Th2 imbalance. *Expert Opin Ther Targets* **2022**, *26* (7), 617−631.
(125) Kasurinen, S.; Happo, M. S.; Rönkkö, T. J.; Orasche, J.; Jokiniemi, J.; Kortelainen, M.; et al. Differences between co-cultures and monocultures in testing the toxicity of particulate matter derived from log wood and pellet combustion. *PLoS One* **2018**, *13* (2), No. e0192453.
(126) Vitucci, E. C. M.; Simmons, A. E.; Martin, E. M.; McCullough, S. D. Epithelial MAPK signaling directs endothelial NRF2 signaling and IL-8 secretion in a tri-culture model of the alveolar-microvascular interface following diesel exhaust particulate (DEP) exposure. *Part. Fibre Toxicol.* **2024**, *21* (1), 15.
(127) Haynes, W. M.. CRC Handbook of Chemistry and Physics. 92nd Edition. *Anticancer Res.*; CRC Press, 2012; Vol. *32*, pp 2220.

https://doi.org/10.1021/acs.chemrestox.5c00206
Chem. Res. Toxicol. 2025, 38, 1708−1728